AIChE
JOURNAL

Improving the load flexibility of industrial air separation units using a pressure-driven digital twin

Robert Kender[1] | Felix Rößler[1,2] | Bernd Wunderlich[2] | Martin Pottmann[2] | Ingo Thomas[2] | Anna-Maria Ecker[2] | Sebastian Rehfeldt[1] | Harald Klein[1]

[1]Department of Energy and Process
Engineering, TUM School of Engineering and
Design, Institute of Plant and Process
Technology, Technical University of Munich,
Garching, Germany

[2]Linde GmbH, Linde Engineering, Pullach,
Germany

Correspondence
Robert Kender, TUM School of Engineering
and Design, Department of Energy and
Process Engineering, Institute of Plant and
Process Technology, Technical University of
Munich, 85748 Garching, Germany.
Email: robert.kender@tum.de

Funding information
German Federal Ministry of Education and
Research (BMBF), Grant/Award Number:
Kopernikus SynErgie (FKZ 03SFK3E1-2).

Abstract

Air separation units are one of the prime examples for studies on demand side
management and (non-)linear model predictive control due to their high power con-
sumption and energy storage potential. These plants separate ambient air into its
main components, nitrogen, oxygen, and argon, by means of cryogenic distillation at
different pressure levels. Approximately two thirds of the industrially operated air
separation units consider the separation of argon either as a value product or for rea-
sons of energy efficiency. However, most of the studies in literature neglect the sep-
aration of argon since this requires additional equipment, increases the heat and
process integration and, thus, the complexity of process control. In this work, a digital
twin of an air separation unit with argon system is used to analyze and to improve
load change procedures. Moreover, the potential of applying the digital twin as a soft
sensor is demonstrated.

KEYWORDS
air separation, digital twin, flexible operation, pressure-driven simulation, soft sensor

1 | INTRODUCTION

Currently, one of the main global challenges in industry and politics is
climate change. A main contribution toward a more sustainable future
is the adaption of energy-intensive production processes, for instance
chemical plants, to the volatile availability of renewable energy
sources. Thus, the load flexible operation of air separation units
(ASUs) is investigated in the Kopernikus project SynErgie FlexASU.
This project is a collaboration of industry and several universities in
Germany. FlexASU project partners are Linde Engineering, MAN
Energy Solutions, the Technical University of Munich, RWTH Aachen
University, the University of the Federal Armed Forces in Munich and
the Technical University of Berlin. ASUs separate air into its main
components nitrogen (N_2), oxygen (O_2), and argon (Ar) by means of
cryogenic distillation. These plants are often used for studies

concerning the flexibilization of plant operation as their high energy
demand for the compression of air and the possibility to store energy
with high energy density using cryogenic liquids entail an outstanding
flexibilization potential.[1–8]

A key factor toward efficient, flexible operation is
energy-optimized operational planning. Depending on the considered
time period, either process control (short-term) or scheduling (long-
term) aspects are of interest. For long-term operational planning,
demand side management (DSM) is widely used. Here, surrogate plant
models are subjected to mixed-integer optimization to minimize oper-
ating expenditures with regard to time-sensitive electricity prices.[9,10]
As one of the first, Daryanian et al.[11] apply DSM to an ASU. They use
a linear dependency of product flow on the electricity consumption
without considering dynamic plant behavior in detail. However, only
N_2 and O_2 are considered as products. Current surrogate models are

more complex as their data basis is either derived from historical plant data[10,12-15] or from steady-state simulation of various operating points.[13-23] Here, dynamic plant behavior is represented by optimization constraints, for example, the maximum load change velocity.[10,13,14,16-19] The main focus of literature is on less complex plant topologies such as O_2[11,16-18,23] or N_2 plants.[10,15,19,22] Only a few of these studies consider the additional separation of Ar.[12-14,20,21]

Due to the increasing share of renewable energies in the energy supply, short-term fluctuations in the energy market can be observed. Thus, advanced process control (APC) concepts based on nonlinear model predictive control (NMPC) are necessary to efficiently operate an ASU in this dynamic environment. Therefore, it is necessary to combine short-term ASU operation with operational planning. To cope with this task, two different paradigms can be applied: bottom-up and top-down. The top-down paradigm follows a hierarchical approach in which DSM problems are solved offline to calculate optimal setpoints for the process control layer. Here, scale-bridging models (SBMs) are used. These rely on low-order representations of closed-loop process dynamics relevant for scheduling and, thus, bridge the time scales between the long-term scheduling calculation and short-term process control. Examples for the usage of SBMs for ASUs can be found in literature.[10,15,24-27] However, these studies are conducted using a N_2 plant. An example of the bottom-up approach is the economic NMPC (eNMPC). Here, dynamic optimization of a rigorous plant model (control model) with an economic target function is performed. The operational planning as well as the input variables for the process control layer are adjusted according to the optimization result with regard to energy-optimal operation. Examples for the application of eNMPC to ASUs in literature use either O_2 plants[28,29] or N_2 plants.[30,31] Caspari et al.[32] compare both paradigms using the example of a N_2 plant. Vinson[33] considers the additional separation of Ar reviewing model predictive control (MPC) strategies for air separation. Moreover, Blum et al.[34] present a model-based deep reinforcement learning controller which is applied to a single control loop of an ASU with Ar production.

Besides the development of complex NMPC strategies, the simulation of isolated load change procedures of an ASU can be found in literature as well. Engl et al.[35] and Kröner et al.[36] publish studies regarding the optimization of a single load change procedure (operating range: 60%–100%) of an ASU with Ar separation. However, considering flexible plant operation, the complete load range is of interest to investigate start-up processes or sudden plant shutdowns. For instance, Caspari et al.[29,37] optimize the start-up procedure of a single N_2 purification column and a N_2 plant. Wunderlich[38] develops a highly detailed pressure-driven model for columns with structured packings. This model is able to simulate the whole operating range of the thermally coupled double column, the centerpiece of every ASU. Kender et al.[3,4] refine this model and use it for the investigation of start-up and shutdown procedures. Klein et al.[5] extend this model with the remaining unit operations, for instance the main heat exchanger (MHEX) according to Rößler et al.,[39] to investigate start-up procedures of O_2 plants. Based on this work, Kender et al.[1] present a digital twin (DT) concept for flexible ASUs. Here, industrially relevant load

changes, in particular a shutdown and cold restart as well as a hazard analysis of the considered O_2 plant, are presented. Kender et al.[40] include the additional separation of Ar and simulate a warm start-up of this ASU topology. Furthermore, Miller et al.[41] investigate a cold restart of an ASU with Ar system. After validating their models with plant data, they conduct dynamic simulation studies with various measures to reduce the cold restart time. They discover that additional storage vessels, which collect the liquid that drains from the argon column during shutdown and allow to reintroduce this liquid during the subsequent restart, reduce the start-up time by ≈80%. Cao et al.[42] evaluate the economic benefit of preemptive control action in advance of an upcoming load change for an ASU with Ar separation. They conduct various dynamic optimization studies using two demand change scenarios with ±10% gaseous O_2 product load with different degrees of freedom. As one of their findings, it is shown that facilitating the liquid holdup of the pressure column (PC) and the Ar reboiler as degrees of freedom is economically beneficial during a load change. However, they claim that preemptive controls tend to result in operations pushing the system closer to the operating bounds and, thus, requires a careful monitoring of critical parameters.

Apart from studies to improve the flexible and energy-optimal operation of ASUs, Cao et al.[19,43,44] conduct simulations using a N_2 plant as an example to identify potential limitations regarding operational agility (debottlenecking). In addition, Cao et al.[19] identify that the usage of external liquid is a key modification to increase plant flexibility. Furthermore, due to their high number of required separation stages, the distillation columns in ASUs are often used as a subject to model reduction approaches such as compartmentalization,[45] nonlinear wave propagation[46] or collocation.[47] However, only Cao et al.[47] consider the Ar system.

As can be seen by this holistic review of simulation studies on ASUs, only a few consider the additional separation of Ar. Nevertheless, the main part of industrial ASUs (≈2/3 of all ASUs operated by Linde) include the separation of Ar. In addition, large O_2 plants can include an Ar removal column to remove a fraction of the intermediate boiling component Ar and, thus, increase the overall energy efficiency of the O_2 plant.[48,49] Hence, considering the additional separation of Ar is highly relevant for the energy-efficient, flexible operation of industrial ASUs. For studies on plant operation requiring dynamic simulation or even optimization this is particularly challenging. Due to the small boiling point difference between Ar and O_2, a high number of separation stages is required to separate pure Ar from air. In addition, the degree of heat and process integration increases and, hence, a more complex control scheme needs to be applied to these ASUs. Furthermore, since Ar covers only a small fraction of the air feed, a high simulation accuracy is necessary to accurately predict the operation of Ar plants.

In addition, it is shown in literature that the specific utilization of cryogenic liquids is beneficial for plant flexibility. Therefore, based on the concept of Kender et al.,[1] a DT of an industrial ASU with Ar separation is presented in this work and used to investigate the impact of the systematic preemptive shifting of liquid holdup on the load change agility. The remainder of this work is structured as follows: At the

beginning, the basics of the DT concept are briefly described and additional applications, such as the DT's utilization as soft sensor, are introduced. Then, the focus is on the industrial air separation process including the Ar system. The main part focuses on the ASU topology and the increased complexity in terms of required equipment, heat and process integration, control and the resulting challenges for (in silico) operations is highlighted. Then, the innovative *smart liquid management* (SLM) concept is introduced. Eventually, two simulation studies of load change procedures, a 50% turn-down and subsequent 50% turn-up, are discussed, highlighting the benefits of the DT for flexible plant operation.

2 | DIGITAL TWIN OF AN INDUSTRIAL ASU

The DT used in this work is based on the concept of Kender et al.[1] The main idea is that the DT includes a plant model, the *virtual ASU*, which is intended to represent the plant's entire life cycle. The model is implemented in the simulation framework SMI@LE (Simulation Model Infrastructure at Linde Engineering) which provides interfaces to databases of historical plant data and real-time operational data. It is imperative that the data stream is allowed in both directions. This enables, on one hand, the usage of simulation data to improve plant operations and, on the other hand, the continuous refinement of simulation models using plant data. Additional information on SMI@LE can be found in Kender et al.[3,4]

To cope with the different simulation tasks during a plant life cycle, the ability to adjust the virtual ASU's model granularity is crucial. This characteristic is enabled by the modular-hierarchical model structure. For instance, this allows for the replacement of design correlations for column fluid dynamics by linear pressure drop and discharge correlations for faster but less accurate simulations.

A top-down approach is applied for the development of the DT. Currently, a highly detailed dynamic pressure-driven model of an ASU, that is, the finest model granularity, is applied. However, the modular-hierarchical unit operation models allow for the drag and drop replacement of submodels and thus, the adaptation of the model granularity. Further information on the unit operation models, in particular the generic column model, can be found in Kender et al.[1,4] For additional information on the generic heat exchanger model, the interested reader is referred to Rößler et al.[39,50] All unit operation models rely on the pressure-driven approach according to Thomas et al.[51]

In general, the plant life cycle can be divided into two phases: *plant design* and *plant operation*. During the plant design phase, steady-state simulation is predominant. In the *(pre-)sales* and *equipment and process design* stages, steady-state simulation and optimization are used to design the plant for its optimal operating point. In the plant operation phase, dynamic simulation is used to reduce the overall plant *commissioning* time. When the plant is in normal operation, the DT can be used to monitor and optimize the plant behavior (*operation optimization*) on different time scales applying DSM or APC. Figure 1 illustrates the typical plant life cycle of an ASU.
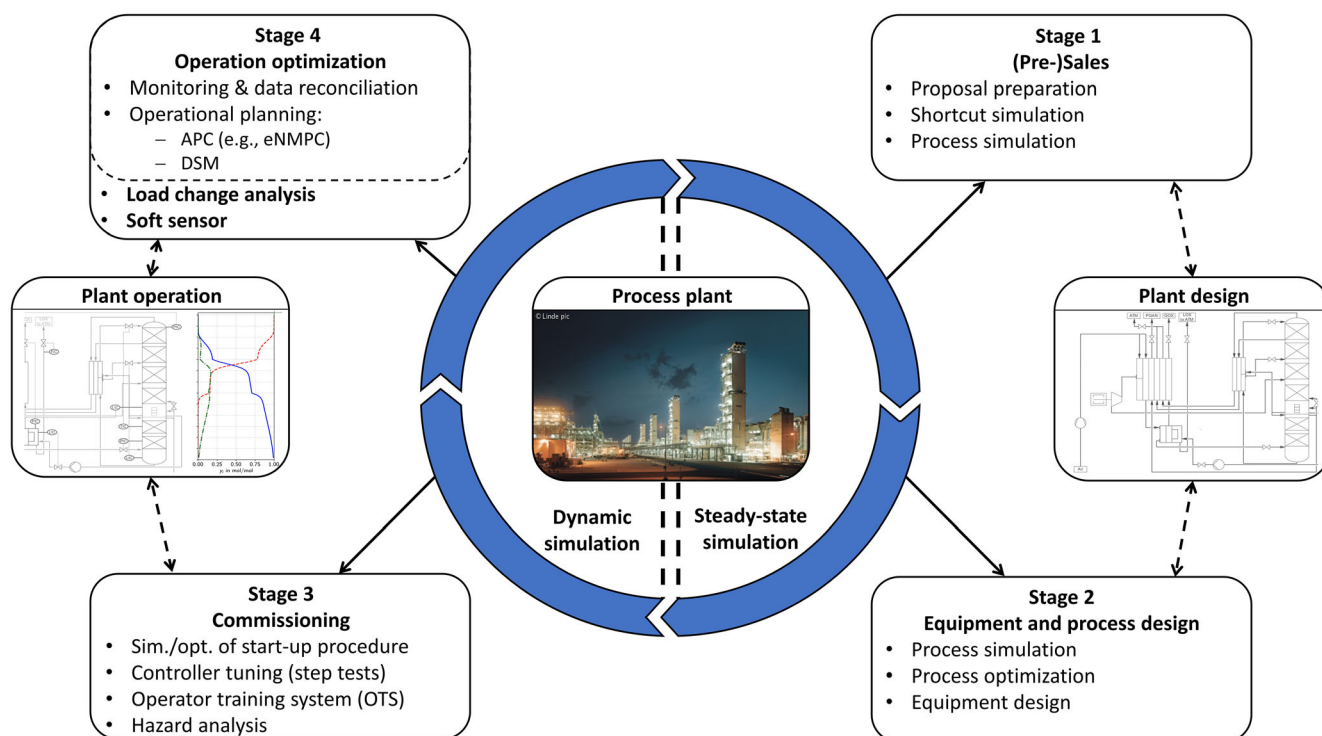

FIGURE 1 Simulation aspects during the life cycle of an ASU according to Kender et al.[1] with the new aspects of load change analysis and soft sensor in stage 4

Further possible applications of the DT in stage 4 are its usage as a *soft sensor* or for the purpose of a *load change analysis* (see Figure 1). In general, the term *soft sensing* refers to approaches and algorithms implemented on computer software-based systems or embedded systems which are used to estimate certain physical quantities or product qualities in industrial processes.[52] Soft sensors can be defined as mathematical models used to predict the behavior of real systems.[53] They can be classified in two main categories, data-driven and model-driven.[54] The focus of this work is on model-driven soft sensors. For more information on data-driven soft sensors, the interested reader is referred to the works of Lin et al.,[54] Kadlec et al.[55] or Jiang et al.[52] The model-driven family of soft sensors is usually based on first principle models, an (extended) Kalman filter, or adaptive observers.[52,55] The DT's application as a soft sensor can be associated with the category of first principle model. The idea of using the DT as soft sensor is as follows. The physical plant's measurement data is used as input or as complementary data for the virtual ASU. Based on the given input (for instance, air feed flow and pressure, product flows, indicated with regular font in Figure 2) the remaining plant state can be calculated. The complementary data (for instance, temperature measurement and O_2-analyzers in the low-pressure column (LPC), indicated with an italic font in Figure 2) can be used to identify faults in the plant by comparing the measured data with the results of dynamic simulations (*bottleneck identification*). Figure 2 compares the available degree of information using the LPC of an ASU as an example.

Using the measurement data from the conventional instrumentation as input, the DT provides full thermodynamic and fluid dynamic information on every column tray, as well as internal column flows and further non-measurable quantities such as the condenser/reboiler duties. This abundance of data can be used to help with the monitoring, control and optimization of industrial processes.[52] However, a common challenge of a soft sensor, which is based on highly detailed dynamic unit operation or plant models is the required computational effort to solve these models. Currently, real-time capability cannot be guaranteed for dynamic simulations of the entire plant using the finest model granularity. However, an application of stand-alone unit operation models such as the double column system as soft sensor is possible. Furthermore, with an increase in computational capabilities the usage of highly detailed dynamic plant models as soft sensor will become more attractive in the future.

In this work, the potential benefits of the DT applied as soft sensor are pointed out in an offline application. Load change procedures are systematically analyzed and improved using non-measurable quantities such as internal column flows. That is, the DT is used for debottlenecking purposes. In the presented case studies, operating and plant design data are used both as input for the basic controller shown in Figure 3 to establish the initial and end states. The remaining plant state is predicted using the virtual ASU (first-principle models).

3 | INDUSTRIAL ASU WITH ARGON SEPARATION

In this section, the air separation process is introduced. Furthermore, the increased complexity in terms of equipment, control, as well as heat and process integration related to the separation of Ar is
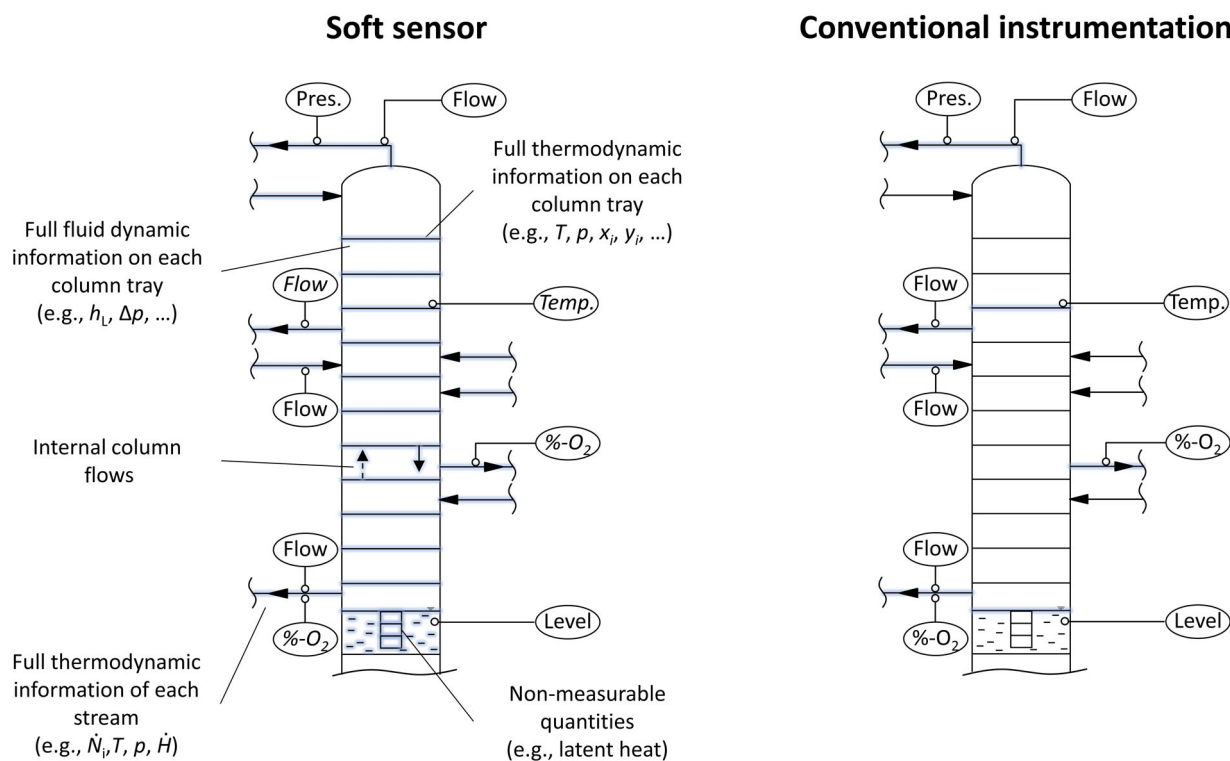

FIGURE 2 Available data (highlighted): DT used as a soft sensor (left) and conventional instrumentation (right)

explained in detail. In addition, the challenges and limitations for load change procedures resulting from this increase in complexity are described.

3.1 | Cryogenic air separation process

ASUs separate air into its main components N_2, O_2 and Ar by means of cryogenic distillation. The molar composition of air is as follows: $y_{N_2,Air} = 0.78118$, $y_{O_2,Air} = 0.20950$, and $y_{Ar,Air} = 0.00932$.[38]

Figure 3 illustrates a process flow diagram of the ASU topology with Ar separation. Here, the purification of air in molecular sieve adsorbers is not considered. The purified air is compressed to a pressure level of 0.6 MPa by the main air compressor ((1)). The pressurized air (GAP, gaseous air pressurized) is then split into two streams. Both streams enter the MHEX ((2)). The main air stream is cooled down over the full length of the MHEX until it is partially liquefied. The partially liquefied main air stream is then fed into the PC ((5)). The second and significantly smaller air stream uses only part of the length of the MHEX, is then expanded in a turbine ((3)) and is fed directly to the LPC ((6)). The expansion provides the refrigeration duty required for the cryogenic air separation.

The centerpiece of an ASU is the thermally coupled distillation system, the double column.[48] It includes the PC at the bottom, the condenser/reboiler or main condenser (MC, (7)), and the LPC on top. Here, air is separated into two of its main components: N_2 and O_2. The third component, Ar, cannot be separated in this column system but in the additional distillation columns in the Ar separation part. The

PC operates at a pressure level of $p_{PC} \approx 0.5$ to 0.6 MPa, whereas the LPC operates at $p_{LPC} \approx 0.12$ to 0.16 MPa. In the topology shown in Figure 3, both columns are sieve tray columns with tray numbers of $n_{tray,PC} \approx 50$ and $n_{tray,LPC} \approx 100$, which are typical values for ASUs.[1] The columns are thermally coupled via the MC, where the condensation of pure N_2 at the top of the PC at elevated pressure provides the heat duty required to evaporate the liquid O_2 in the sump of the LPC. The condensed liquid N_2 (LIN) is used as reflux for both columns. The O_2-enriched liquid air at the bottom of the PC (crude liquid oxygen pressurized, CLOP) is used as liquid feed for the LPC. Both streams, CLOP and LIN, are further cooled in an additional heat exchanger, the subcooler (SC, (4)), before they are fed to the LPC.

The main products of this ASU topology are gaseous O_2 (GOX), gaseous N_2 (GAN) and liquid Ar (LAR). Furthermore, an impure N_2 stream (crude gaseous nitrogen, CGN) is withdrawn from the LPC and vented to the atmosphere (ATM). In addition, a small amount of liquid O_2 (LOX) is withdrawn from the bottom of the LPC as a purge stream. Pressurized gaseous N_2 (PGAN) from the top of the PC is used as a seal gas or product stream.

In order to produce pure Ar, two additional distillation columns, the crude Ar (CAC, (8)) and pure Ar (PAC, (10)) column are required to remove O_2 and N_2 from the Ar column feed which is withdrawn from the LPC (crude gaseous oxygen, CGO). Both, the CAC and the PAC are typically columns using high efficiency structured packings.[56] The Ar column feed CGO is an O_2-rich mixture, containing a relatively high amount of Ar and traces of N_2. The purpose of the CAC is to separate O_2 from the Ar column feed CGO. Due to the low boiling point difference between O_2 and Ar (see Figure 5) a high number of theoretical
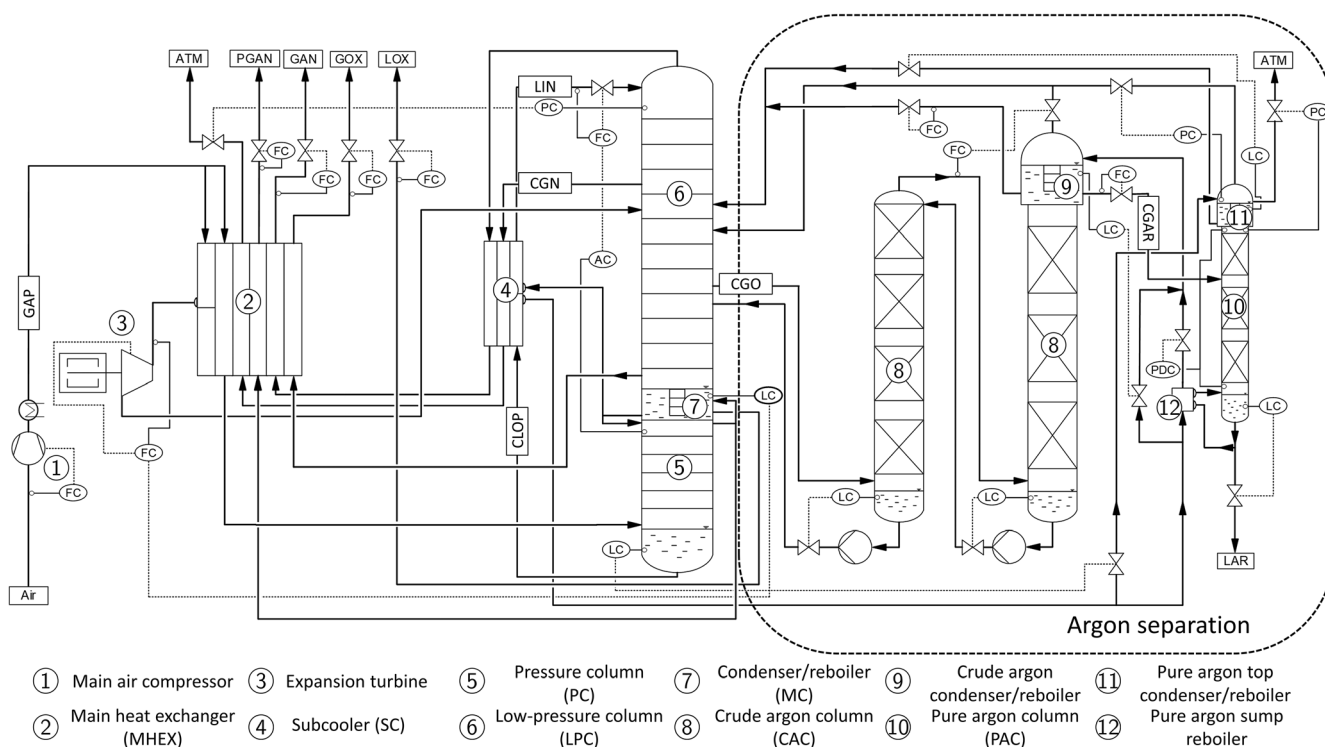

FIGURE 3 ASU topology—process flow diagram of an industrial ASU with Ar separation including the basic control layer

trays ($n_{\text{tray,CAC}} \approx 200$) is required in the CAC. Here, the CAC is split into two columns due to height limitations. The purpose of the PAC is to remove the remaining traces of N_2 from the crude Ar stream crude gaseous argon (CGAR), the top product of the CAC. Here, additional $n_{\text{tray,PAC}} \approx 50$ theoretical trays are required. The tray numbers for the columns required for this simulation task are summed up in Table 1.

Moreover, two additional condenser/reboilers and another reboiler are required for the separation of Ar increasing the complexity of the ASU's thermal integration. The subcooled CLOP stream is split in two, before one part is eventually fed to the crude Ar condenser/reboiler (⑨), whereas the other part is fed to the pure Ar condenser/reboiler (⑪). In the crude Ar condenser/reboiler, while partially evaporating the CLOP at elevated pressure, the crude Ar is condensed, generating the reflux for the CAC. Prior to that, the liquid influx for the crude Ar condenser/reboiler is further split. One part of this CLOP is subcooled, evaporating the liquid Ar in the pure Ar sump reboiler (⑫) to generate vapor flow in the PAC. As for the liquid reflux of the PAC, the other part of the first CLOP split is partially evaporated in the pure Ar top condenser/reboiler. The increasing complexity due to the additional Ar separation (see Figure 3, dashed line) is explained in detail in Section 3.2.

In addition, the base control layer of the ASU is illustrated in Figure 3. The main products, GOX and GAN, as well as the purge stream LOX and the seal gas PGAN are subject to flow control. The valve strokes h_v of the corresponding product valves are adjusted to achieve the desired amount of flow. Furthermore, the main air flow, the amount of the Ar column feed CGO flow as well as the O_2-enriched liquid flow from the crude Ar condenser/reboiler are subject to flow control. To obtain the desired air flow, the discharge pressure of the main air compressor is adjusted. The controllers required for the separation of Ar are explained in the following section. Furthermore, the N_2 concentration of the LIN reflux for the PC and the LPC is controlled by a cascade of an AC and a FC. A PDC controls the pressure difference in the PAC as a measure of the column load by adjusting the CLOP split to influence the pure Ar sump reboiler duty and, thus, the reboil ratio for the PAC. The remaining controllers are level controllers. Except for the MC and the crude Ar condenser/reboiler level, the liquid outflow is adjusted to control the levels. For the MC level, a cascade controller is used, adjusting the turbine flow and, hence, the refrigeration duty to meet the MC level requirements. For the crude Ar condenser/reboiler the liquid inflow is adjusted to control the level. The first order plus time delay method is used as a basis for controller tuning.[57] Further information on the process of air separation can be found in Häring[58] or Hausen and Linde.[59]

TABLE 1 Required (theoretical) tray numbers for PC, the LPC, the CAC, and the PAC

Column	Number of (theoretical) trays n_{tray}
PC	50
LPC	100
CAC	200
PAC	50

3.2 | Ar separation

As already mentioned, air contains only a small quantity of Ar ($y_{\text{Ar,air}} = 0.00932$), which indicates that the additional separation of Ar increases the complexity of the ASU in terms of the equipment required. Furthermore, the additional heat and process integration of the Ar system limits the load change agility. In addition, the dynamic simulation of an ASU with Ar separation is numerically highly challenging, which is explained later in this section. Figure 4 visualizes the Ar separation.

The Ar column feed CGO is withdrawn at a suitable location of the LPC where the intermediate boiler Ar is accumulated. Figure 4 also shows the typical vapor concentration profile of the LPC including the location and composition of the CGO stream. The Ar column feed CGO typically consists mainly of O_2, an increased amount of Ar and traces of N_2.

Figure 5 shows the pressure of vaporization curves of N_2, Ar and O_2. As can be seen, the difference between the boiling point temperatures T_{boil} of Ar and O_2 is small ($\Delta T_{\text{boil,Ar,O}_2} \approx 2.85$ K) resulting in the high number of theoretical trays required to separate O_2 from the CGO stream. Since the Ar column feed CGO is withdrawn from the LPC which operates at $p_{\text{LPC}} \approx 0.12$ to 0.16 MPa, high separation efficiency and a small pressure drop in the used packings in the CAC are crucial. Due to the large quantity of O_2 in the CGO stream, the CAC is operated close to total reflux.[56]

The liquid reflux is generated in the crude Ar condenser/reboiler condensing most of the CGAR vapor while partially evaporating a part of the O_2-rich CLOP stream at elevated pressure. Thus, the amount of liquid reflux for the CAC is strongly dependent on the temperature difference $\Delta T_{\text{cond/reb,CAC}} = T_{\text{dew,CGAR}} - T_{\text{bub,CLOP}}$ of the two fluids at each side of the crude Ar condenser/reboiler, which is the driving force for the condensation process. Both temperatures are dependent on the pressure p and the composition z_i of the corresponding fluid.

On the reboiler side, the pressure p is the key parameter to influence the bubble point temperature $T_{\text{bub,CLOP}}$ since the composition of CLOP is almost constant over a wide operating range. The amount of the Ar column feed CGO is controlled implicitly by adjusting the outflow of the partially evaporated CLOP stream leaving the crude Ar condenser/reboiler. The amount of vapor leaving the crude Ar condenser/reboiler is used to adjust the pressure in this vessel and, thus, the bubble point temperature $T_{\text{bub,CLOP}}$. This directly impacts the amount of liquid reflux in the CAC, which is decisive for the flow resistance of the vapor in the CAC and thus the amount of CGO flow. The liquid outflow of the crude Ar condenser/reboiler is subject to flow control. The liquid inflow into this condenser/reboiler is used to control its level.

On the condenser side, the composition of CGAR is crucial. On the one hand, it is essential that the amount of N_2 in the Ar column feed CGO is kept at a considerably low level (see Figure 4; $y_{\text{N}_2,\text{CGO}} = 2.4 \times 10^{-5}$). Since N_2 is the low boiling component in air, an increase in N_2 in the Ar column feed CGO is equivalent to a subsequent reduction in the dew temperature $T_{\text{dew,CGAR}}$ of the CGAR. Thus, the temperature difference $\Delta T_{\text{cond/reb,CAC}}$ decreases with an
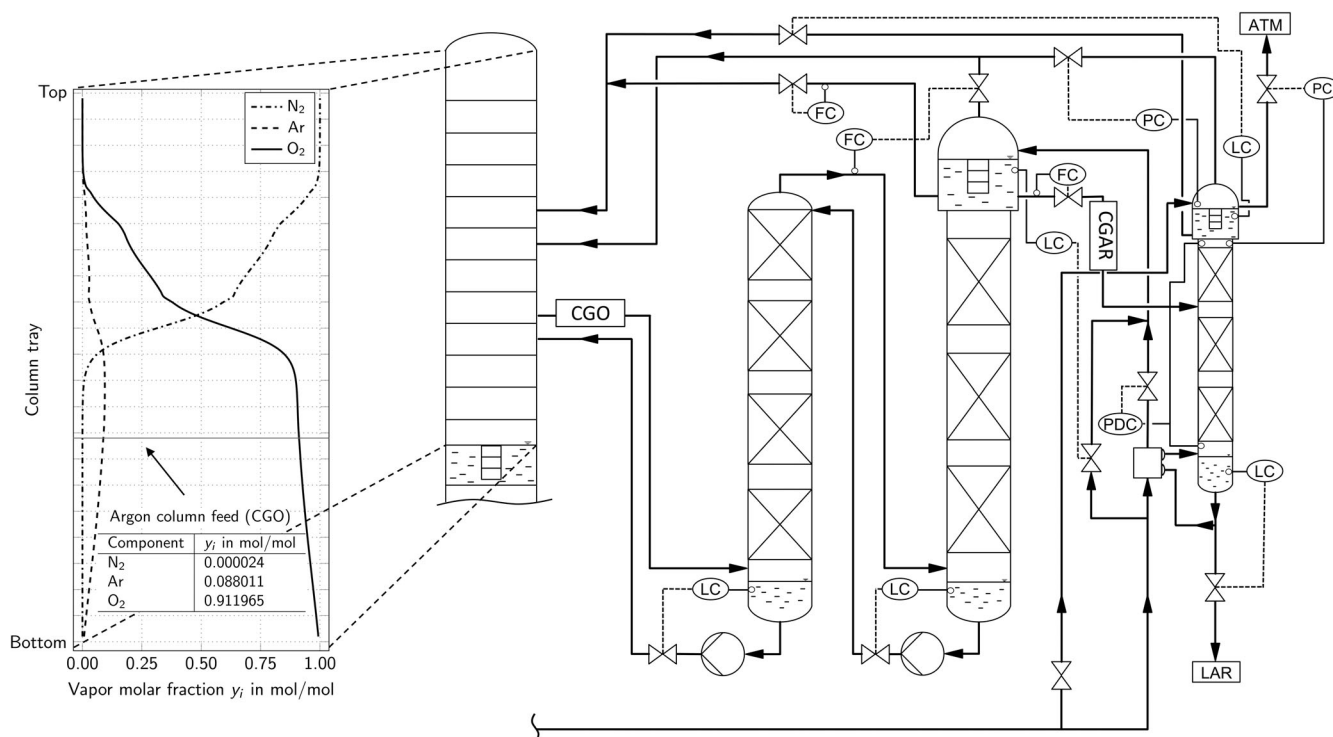
FIGURE 4 Visualization of the topology of the Ar system and of a typical vapor concentration profile of the LPC including the location and composition of the Ar column feed CGO
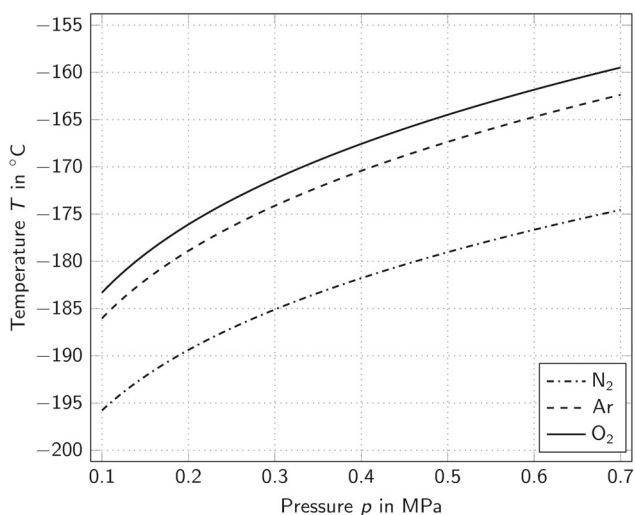

FIGURE 5 Pressure of vaporization curves of the main air components

TABLE 2 Purity constraints for the ASU products

Product stream	Threshold of O_2 vapor molar fraction y_{O_2}
CGAR (LAR)	≤5 ppm
PGAN	≤5 ppm
GAN	≤5 ppm
GOX	≥0.995

increasing amount of N_2. At a certain threshold the dew temperature of the CGAR drops below the bubble temperature of the CLOP on the reboiler side ($T_{dew,CAr} \leq T_{bub,CLOP}$) leading to the disappearance of the liquid reflux due to a reversal of the heat flux $\dot{Q}_{cond/reb,CAC}$. That is, with too much N_2 in the Ar column feed CGO, the Ar system collapses. This event is to be prevented as it entails a prolonged product loss during the restart of the Ar system. On the other hand, a high purity of the Ar product LAR is required. The maximum amount of O_2

in the LAR in the demonstrated case is specified with $x_{O_2,LAR} = 5$ ppm.[60] However, an excess of O_2 in the Ar column feed CGO does not lead to a collapse of the CAC liquid reflux due to the similar boiling point temperatures of Ar and O_2. Further purity constraints for the products of the considered ASU are shown in Table 2.

Maintaining the high purity requirements during a load change procedures is highly challenging for an ASU with Ar separation. It is required to limit the maximum load change rate to prevent, for instance, temporary changes in the fluid dynamic conditions inside the columns, which affect the separation efficiency, to be able to adhere to the purity constraints at all time.

In addition, there is a strong dependency of the GOX product on the CGO stream and vice versa. This further emphasizes the high degree of process integration of an ASU with Ar separation. To visualize the impact of GOX production on the Ar system, a steady-state parameter study of the GOX product flow on the GOX and LAR product purities is displayed in Figure 6.

Here, the amount of GOX product flow is slightly varied around the operating point (from $\delta = -1.2\%$ to $\delta = 0.5\%$), to represent a
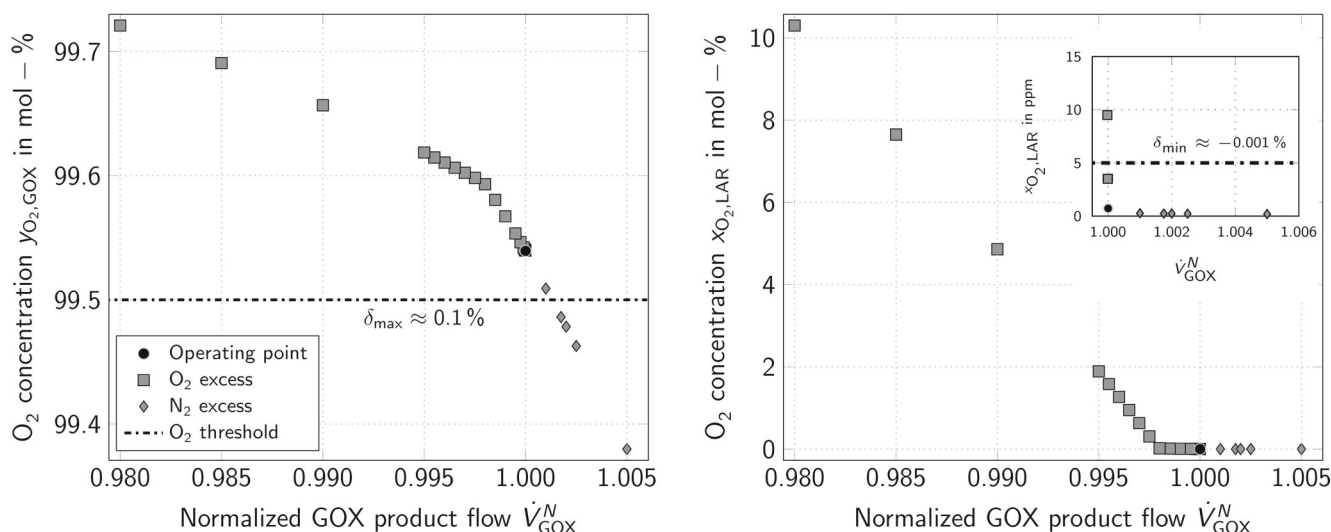
FIGURE 6 Variation of normalized GOX product flow—impact on GOX product (left) impact on LAR product (right)
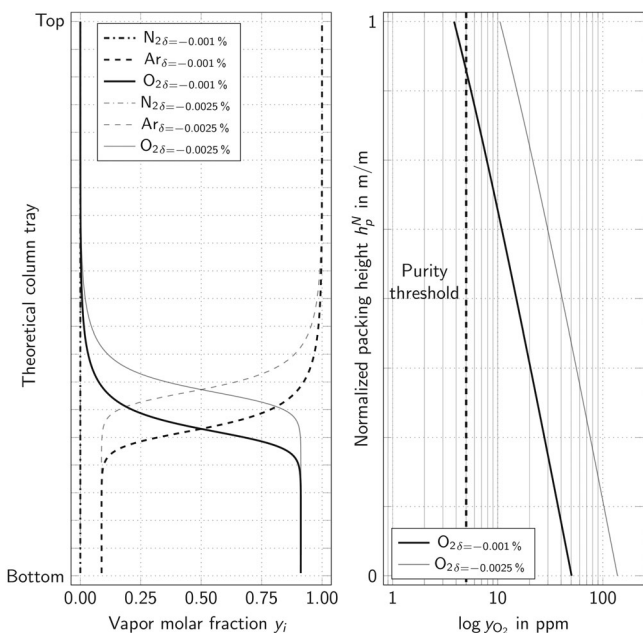

FIGURE 7 Variation of normalized GOX product flow—impact on the CAC concentration profile

disturbance in plant operation. This flow variation impacts the GOX product purity. A flow increase leads to a decrease in purity and vice versa. The flow increase is limited by the purity threshold of the GOX product (see Figure 6, left diagram). Here, the limit of the flow deviation is $\delta_{max} \approx 0.1\%$. A further increase in GOX flow violates the purity threshold at first and leads eventually to the collapse of the Ar system due to an increased amount of N_2 in the Ar column feed CGO.

The possible reduction in GOX flow is limited by LAR product purity as visualized in Figure 6 on the right. Here, only a deviation of $\delta_{min} \approx -0.001\%$ is possible without violating any constraint. This indicates that at the considered operating point the maximal amount of

LAR is withdrawn. Figure 7 shows the vapor concentration profile of the CAC at $\delta = -0.001$ and $\delta = -0.0025\%$ on the left and the O_2 vapor molar fraction graph of the uppermost CAC packed bed of both cases on a logarithmic scale on the right.

As can be seen in the left diagram, the minimal deviation in GOX product flow has a tremendous effect on the separation of O_2 from the Ar column feed CGO although the changes in the composition of the Ar column feed CGO ($|\Delta y_{O2,CGO}| = 6.05 \times 10^{-5}$) are minimal. The concentration profile of the CAC is significantly shifted upwards. Thus, in the case of $\delta_{-0.0025\%}$ there are insufficient trays to purify the CGAR to the required value. The logarithmic scale (see Figure 7, right diagram) reveals that even in the uppermost packed bed there is no pinch but an ongoing separation of Ar and O_2.

Eventually, the traces of N_2 are separated from the CGAR in the PAC. The N_2-rich fraction at the top of the PAC is vented to the atmosphere whereas the pure Ar product LAR is withdrawn in liquid form at the bottom of the PAC. Although the separation of the N_2 traces is a comparatively simple task, it still requires another $n_{tray,PAC} \approx 50$ as well as one additional condenser/reboiler and another reboiler to provide the required boil-up and reflux for this column. Thus, the complexity of process integration is further increased. The amount of LAR product is the result of the level control applied to the sump of the PAC. The reboil ratio of the PAC is controlled via the pressure difference control of this column. This kind of control can be applied due to the almost constant composition of the CGAR top product of the CAC (feed for the PAC) when the plant is operated in its operating envelope. Thus, the effects of changing composition on the pressure drop can be disregarded and the pressure difference is a reliable indication for vapor flow in this column. The top of the PAC is subject to pressure control manipulating the N_2-rich vent stream to the atmosphere. The pure Ar top condenser/reboiler is also subject to level and pressure control.

It is evident that the additional separation of Ar from air is a complex task. Not only the operation of this kind of plant but also its
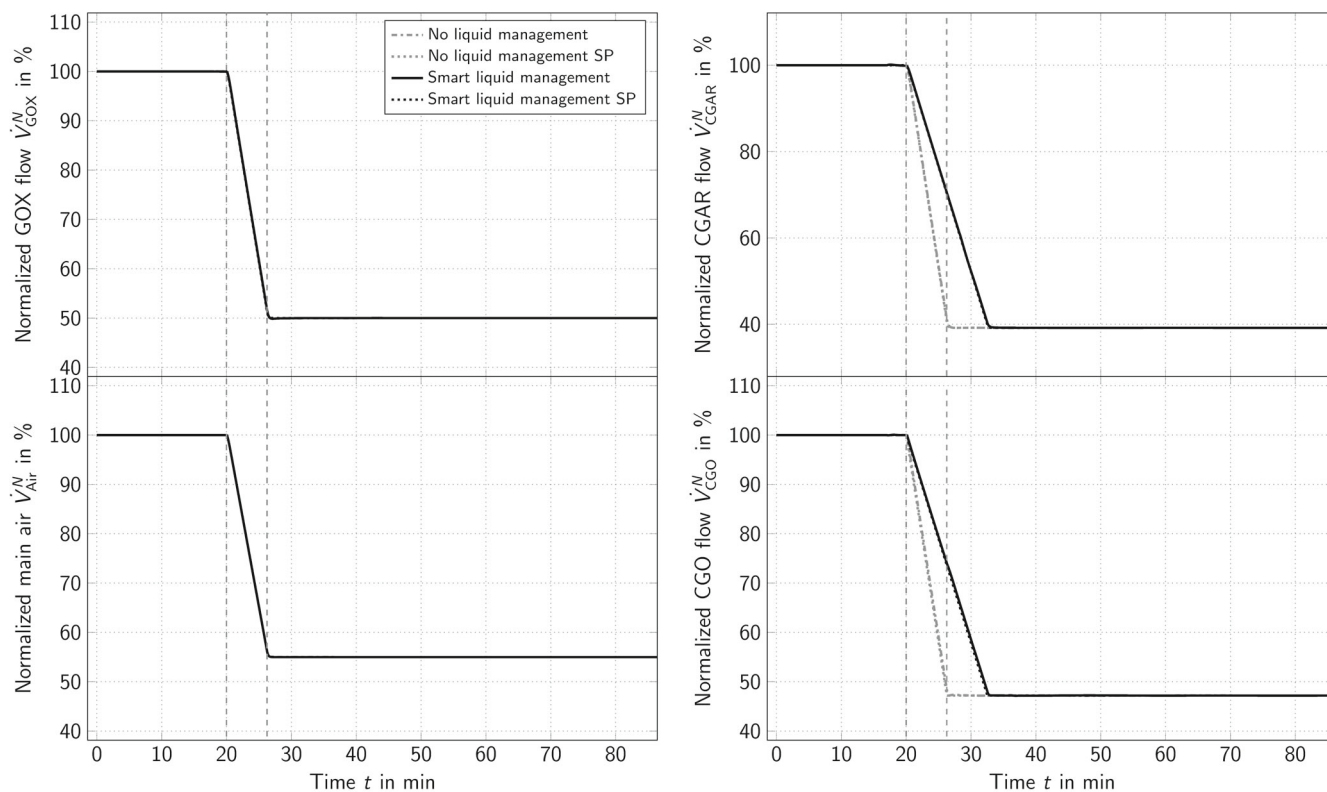
FIGURE 8 Controller inputs for the turn-down: normalized GOX flow (upper left), normalized air flow (lower left), normalized CGAR flow (upper right) and normalized CGO flow (lower right)

dynamic simulation is challenging. The large number of required theoretical trays $n_{\text{tray,total}} \approx 400$ and the accuracy requirements of the heat exchanger models result in a large system of differential and algebraic equations that needs to be integrated over time. In total, the presented virtual ASU contains 2011 differential and 57,325 algebraic equations. In addition, the desired product purities (ppm scale) are challenging for numerical simulation due to the solver tolerances to be used for accurate dynamic simulations. Furthermore, the small difference between the boiling temperatures of Ar and O_2 and the resulting demands on the separation task increase the accuracy requirements for the calculation of fluid properties. Moreover, due to the small quantity of Ar in air, there is a wide range of different magnitudes of process streams which complicates the proper conditioning of the equation system to be solved.[61]

Besides, the high degree of heat and process integration of an ASU with Ar separation increases the complexity of a load change procedure further. Since undesirable effects, such as concentration shifts, as a result of an elevated load change rate, quickly affect the entire ASU state due to degree of integration, the importance of limiting the load change rate as a precautionary measure is emphasized yet again. However, since flexible operation requires fast load changes, appropriate measures are required to cope with these challenges. Therefore, in the following section the SLM concept presented, which allows to increase the load change rate of an ASU with Ar production without violating purity requirements.

4 | SMART LIQUID MANAGEMENT

As already outlined in the work of Miller et al.[41] and Cao et al.,[19,42] the (preemptive) utilization of cryogenic liquids during a load change procedure allows for an increase of the load change agility and leads to economical benefits. In this work, the SLM concept is developed, which allows for faster load change procedures by preemptively and systematically shifting the liquid in the column sumps of the PC and the CAC during the presented load change procedures in Section 5.

The main idea of the SLM is to prevent a disproportionate accumulation of the excess liquid holdup in the MC by actively distributing it among all column sumps. Thus, the level setpoints of the PC and the CAC are adjusted to their values optimized for part-load operation. These values are determined in additional dynamic simulations replacing the level controller of the corresponding column sumps with flow controller. The liquid outflows of each sump are ramped down linearly to their part-load value, which leads to the optimal level setpoint. In addition, the changes of these level setpoints are shifted in start time and duration compared to the remaining setpoint changes. The temporal modifications to the level setpoints are a result of additional simulation studies using the S-factor S_i as indicator, which can be used to characterize the separation of the component i on a column tray or in a column section. It is defined as
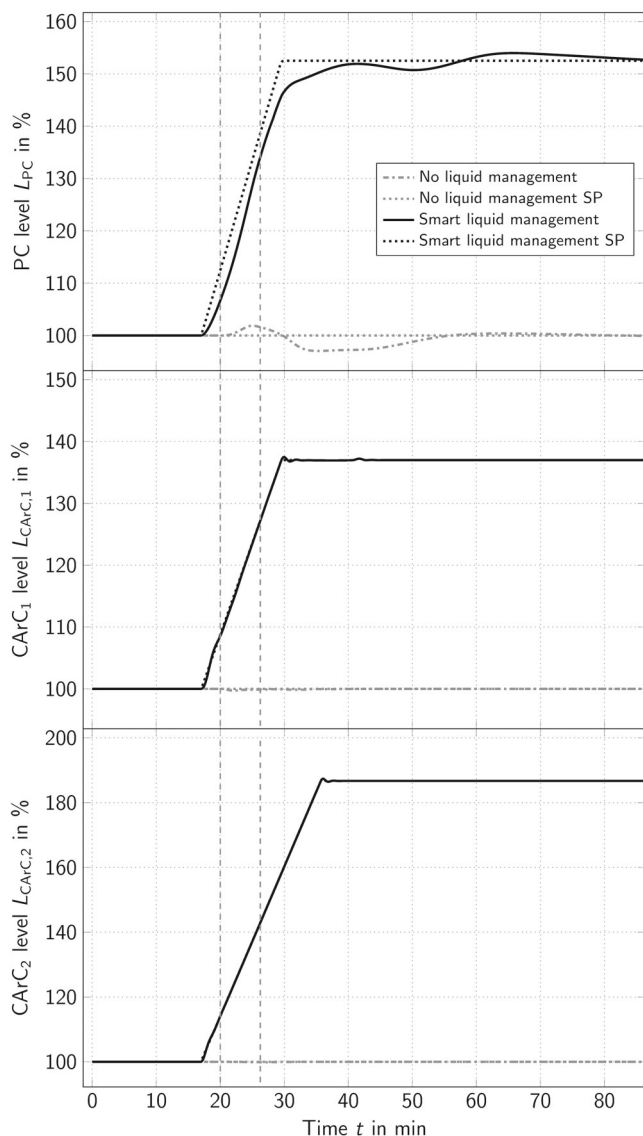
$$S_i = \frac{K_i}{L/G}, \tag{1}$$

FIGURE 9 Controller inputs for the turn-down: PC sump level (top), CAC$_1$ sump level (middle) and sump CAC$_2$ level (bottom)

where K_i represents the vapor–liquid equilibrium ratio of component i, and $\dot{L}/\dot{G}$ is defined as the ratio of liquid to gas flows of the considered tray or column section. This figure can be related to the considerations of Edmister.[62] Its general applicability to the distillation columns in ASUs is shown in Ecker et al.[63] The S-factor quantifies, whether the component i is stripped downwards ($S_i < 1$), rectified upwards ($S_i > 1$) or accumulated in the considered part of the column ($S = 1$). Therefore, it can be used to quantify the effects of adding excess or withholding liquid on the LPC fluid dynamics and separation efficiency. In the SLM concept, the S-factor S_i is mainly used as an early indication of high boiler (GOX) purity in the MC to meet the required purity constraints. This can be achieved by keeping the S-factor S_i, and, thus, the separation efficiency in the LPC column section above the MC constant during the considered load change.

In the next section, the load change procedures of the presented ASU with Ar separation are analyzed and the impact of SLM on the

maximum possible load change rate is evaluated. Based on the abundance of data, these studies are intended to give a detailed insight into the behavior of an ASU with Ar separation during a load change procedure. In addition, as the SLM concept is based on quantities which can hardly be measured in an industrial plant, the additional value of the DT used as soft sensor is emphasized. Thus, further effort required to overcome the challenges of the DT's real-time application is justified.

5 | CASE STUDIES

In the following, two load changes are analyzed via dynamic simulations using the DT: a 50% turn-down and a 50% turn-up scenario. The turn-down starts from the ASU's nominal operating point of 100% load. The term load refers to the amount of main product GOX. The plant load is then reduced to 50% load with the respective adjustments to the remaining plant to ensure optimal part-load operation. To reach the initial state of the turn-down scenario, a warm start-up simulation as explained in Kender et al.[40] was conducted. The initial state of the turn-up corresponds to the final state of the turn-down scenario using the innovative SLM concept (see Section 4). Both scenarios are simulated with a load change rate of 8% min^{-1}, which is significantly faster than a state-of-the-art load change procedure for ASUs with Ar separation. The load change procedures are analyzed to identify challenges and limitations using the abundance of transient simulation data which is available using the DT. For the dynamic simulation of the case studies, a Linde proprietary backward differentiation formulas (BDF) solver was used. Further details on this solver can be found in Kronseder.[64] An integration tolerance of 10^{-4} was chosen by analogy to Kender et al.[1] Furthermore, the Soave–Redlich–Kwong (SRK) cubic equation of state is used by analogy to previous works[1,3,4,38,40] to describe the vapor liquid equilibrium of the ternary mixture N$_2$, O$_2$, and Ar. All the simulations were conducted on a standard workstation with an Intel® Core™ i5-7500 CPU (at 3.40 GHz) with 32 GB RAM.

5.1 | Turn-down

The load change rate of the turn-down is limited due to the adherence to purity constraints. The main challenge during a turn-down procedure is to prevent the loss of high boiler purity (GOX) due to the reduction in main air feed and the resulting decrease in the reboil ratio in the LPC since the MC duty $\dot{Q}_{MC}$ decreases. As a further consequence of the reduced vapor flow through the plant, a temporary excess of liquid holdup can be observed in each column, pouring from each (theoretical) tray into the column sumps. The excess liquid has an increased amount of low boiler of the corresponding column which affects the purity of the high boiler in each column. In addition, the enhanced liquid pouring in the LPC is an additional challenge since it increases the amount of N$_2$ in the liquid flowing down the LPC. This can increase the molar fraction of N$_2$ at the Ar transition, which has to

be prevented to avoid a collapse of the fluid dynamics of the Ar system (see Section 3). However, the purities of the low boiling components N_2 and Ar are not critical during a turn-down procedure. The purity constraints can be seen in Table 2.

Two different cases are compared for the turn-down. In the first case, all controller setpoints for composition, flow and pressure control (see Figure 3 for the control loops) are ramped down linearly to their part-load values. The level setpoints for all condenser/reboilers remain constant at 100% to keep the condenser blocks covered in liquid at all times. In addition, the remaining level setpoints for the column sumps of the PC and both the CACs also remain at their nominal value of 100%. This case is referred to as no liquid management (NLM). In the second case, SLM as described in Section 4 is applied.

For the analysis of the turn-down scenario a time period of 85 min is considered. In the first 20 min the ASU is operated in steady-state at 100% load. Then at $t_{start} = 20$ min the turn-down starts. At $t_{end} = 26.25$ min the required setpoint changes of the entire control layer for part-load operation are finished. The total duration is $\Delta t = 6.25$ min, which corresponds to a load change rate of 8% min^{-1}. The required setpoints for the part-load operation are pre-calculated for an optimal 50% load case in an additional steady-state simulation based on plant design data and all setpoint changes are linear in nature. The term optimal refers to a maximized Ar yield at a minimum power consumption for 50% load. The described load change procedure corresponds to a state-of-the-art feedforward control.

Although not all relevant parameters have reached their final part-load values at $t = 85$ min, this time span is sufficient to describe all relevant aspects of the plant response during the turn-down. In some cases, the final steady-state is obtained after several more hours, for instance the purities of the Ar products CGAR and LAR. However, for a successful load change procedure, it is essential to establish constant flow rates throughout the ASU, especially with regard to column fluid dynamics. The slow concentration shifts do not need to be finished, as the changes remain minor and the purity constraints according to Table 2 are met. The required CPU time for the simulation of both cases is approximately 1 h and 45 min on the used workstation. The relevant setpoint changes for the turn-down are presented in Section 5.1.1. Afterwards, the plant response and the impact of SLM are discussed in Section 5.1.2.

5.1.1 | Controller inputs

In the following, the relevant controller inputs of the turn-down are presented. Figure 8 shows the setpoint changes for the GOX product $\dot{V}_{GOX}$ (upper left), the main air $\dot{V}_{Air}$ (lower left), the CGAR $\dot{V}_{CGAR}$ (upper right) and the CGO flow $\dot{V}_{CGO}$ (lower right) Furthermore, the start and end times of the turn-down are marked with gray dotted vertical lines in all of the following figures. In addition, except for molar fractions, all considered parameters are normalized with respect to their nominal value at 100% load. This is indicated only in the figure captions and the axis labels. In the text, normalized and non-normalized parameters are not distinguished.

In the case of NLM, all presented setpoint changes visualized in Figure 8 start and end at the same time. In the case of SLM, the duration of the setpoint changes for CGO, the Ar column feed, as well as CGAR are twice as long ($\Delta t = 12.5$ min). Figure 9 shows the levels L_{PC}, $L_{CAC,1}$, and $L_{CAC,2}$ and their setpoint changes for the PC and both CACs. The index 1 refers to the first CAC column downstream of the LPC.

For SLM, the setpoint changes of the levels start earlier at $t = 16.875$ min. Furthermore, the duration of the setpoint changes varies. For the PC as well as the CAC$_1$, the end of the setpoint change is at $t = 29.375$ min ($\Delta t = 12.5$ min) and for the CAC$_2$ at $t = 38.625$ min ($\Delta t = 18.75$ min). In addition, Figure 9 illustrates that the level control of the PC shows a higher inertia compared to the
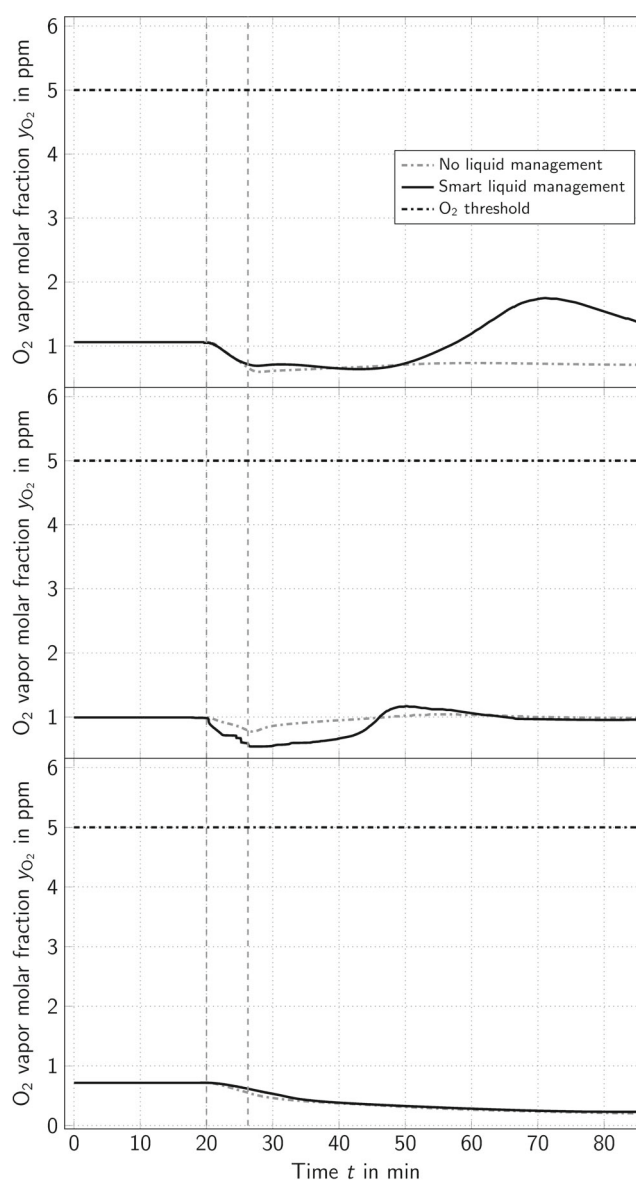
FIGURE 10 Plant response during the turn-down: O_2 vapor molar fraction of the top products of the distillation columns. LPC-GAN (top), PC-PGAN (middle) and CAC-CGAR (bottom)
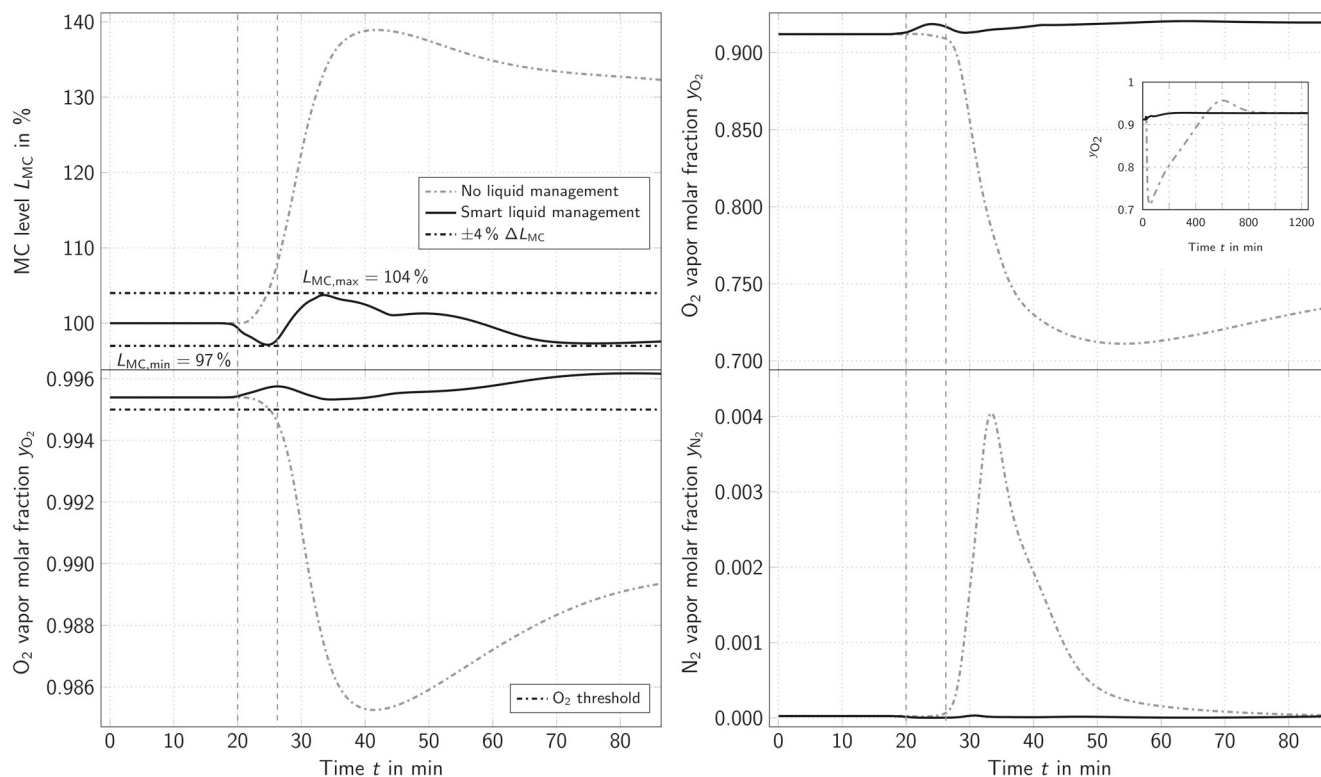
FIGURE 11 Plant response during the turn-down: MC level (upper left), O_2 molar fraction of the GOX product (lower left), O_2 molar fraction of the Ar column feed CGO (upper right), N_2 molar fraction of the Ar column feed CGO (lower right)

level controls of the CAC. As shown in Figure 3, the outflow of the CAC sumps and thus the level are controlled via pumps, which allows for a faster control compared to the PC level. The setpoint changes of the remaining control loops (see Figure 3) to establish optimal part-load operation, for instance, GAN product decrease or LPC pressure adjustment, are not of particular importance for this case study and therefore not visualized.

5.1.2 | Plant response

In this section, the plant response of the turn-down is presented. It is structured as follows: first, the low boiling components N_2 at the top of the PC and the LPC as well as Ar at the top of the CAC are considered. Then, the focus is on the lower part of the LPC including the Ar column feed CGO and the high boiler O_2 (GOX) in the MC. Afterwards, the response of the Ar system is presented before LPC fluid dynamics are discussed in detail.

Low boiling components
Due to the temporarily increased reflux during the turn-down, the purities of the low boiling components N_2 and Ar are not critical. This is illustrated in Figure 10. Here, the O_2 vapor mole fractions $y_{O_2,GAN}$, $y_{O_2,PGAN}$, and $y_{O_2,CGAR}$ of the process streams GAN (low boiler LPC), PGAN (low boiler PC) and CGAR (low boiler CAC) are plotted over time.

For all three streams, a maximum O_2 content of 5 ppm is not exceeded. The difference of the O_2 purities of GAN and PGAN between NLM and SLM can be explained with the different flow conditions inside the PC and the LPC, which are caused by the different handling of the excess liquid holdup in both cases.

LPC—lower part
Figure 11 shows the response of the lower part of the LPC, which contains the most critical parameters during the turn-down scenario. The level of the MC L_{MC} (top) and the O_2 vapor molar fraction of the GOX product $y_{O_2,GOX}$ (bottom) are shown on the left side, whereas the Ar column feed CGO vapor molar fractions ($y_{O_2,CGO}$ at the top and $y_{N_2,CGO}$ at the bottom) are shown on the right side.

The graphs on the left side of Figure 11 illustrate the main challenges of the turn-down procedure. Without transferring the excess liquid holdup to the corresponding column sumps, it is all accumulated in the MC, causing the level to rise significantly (see 11 upper left). Looking at NLM, the MC level rises to a maximum of $L_{MC,max} = 139\%$ at $t = 41.8$ min before it slowly decreases again. Applying SLM, the MC level L_{MC} initially decreases due to the fact that the level setpoints are changed on purpose prior to the remaining load change procedure (see Figure 9). However, the variation of the MC level L_{MC} remains in a range of ±4%, which is not safety critical as the condenser is still covered with liquid sufficiently.

The lower left side of Figure 11 visualizes the molar fraction $y_{O_2,GOX}$ of the GOX product. In the case of NLM, at $t_{start} = 20$ min, the

O_2 vapor molar fraction $y_{O_2,GOX}$ starts to decrease. The constraint for the product purity $y_{O_2,GOX} \geq 0.995$ is violated at $t = 25.07$ min. At $t = 41.42$ min, the minimum O_2 vapor molar fraction of $y_{O_2,GOX,min} = 0.985$ can be observed. Afterwards, $y_{O_2,GOX}$ increases and the purity requirement is eventually met again at $t \approx 5$ h which is not displayed. With SLM, the purity constraint for the GOX product is met at all times. This can be explained by using the composition of the liquid holdup in the sump of the CAC_1 (see Figure 12) and the S-factor of Ar S_{Ar} at the first column tray above the MC at the bottom of the LPC (see Figure 13) which is explained later in this section.

At the lower right of Figure 11, the graph of the N_2 vapor molar fraction $y_{N_2,CGO}$ of the Ar column feed CGO illustrates another difficulty of a rapid turn-down procedure. As can be seen in the case of NLM, $y_{N_2,CGO}$ increases rapidly after the setpoint changes are completed at $t_{end} = 26.25$ min. At $t = 33.53$ min a maximum of the N_2 molar fraction of $y_{N_2,CGO} = 0.00403$ is reached. This can be explained with the increased molar fraction of N_2 in the excess liquid holdup, which is pouring down the LPC to accumulate in the MC. During the presented turn-down the increased amount of N_2 in the Ar column feed CGO is not sufficient to significantly impact the crude Ar condenser/reboiler and, thus, the liquid reflux of the CAC. However, a larger N_2 intake could occur under similar operating conditions leading to collapsing fluid dynamics of the Ar system. To avoid this, SLM can be applied resulting in an almost constant vapor molar fraction $y_{N_2,CGO}$ throughout the turn-down.

The graph of the O_2 vapor molar fraction $y_{O_2,CGO}$ of the Ar column feed CGO (upper right) is similar to the graph of the O_2 vapor fraction of the GOX product $y_{O_2,GOX}$. In addition, a small excerpt is shown in this diagram, which illustrates the course of $y_{O_2,CGO}$ over 1350 min. It shows that for both cases, a constant graph is eventually reached at $t \approx 200$ min $= 3.33$ h for SLM and $t \approx 1000$ min $= 16.67$ h using NLM. Thus, a steady-state for the ASU is reached, as a constant course of $y_{O_2,CGO}$ requires stationary LPC fluid dynamics. A requirement for this is a constant MC duty $\dot{Q}_{MC}$, which is representative for the overall plant state. However, using NLM, the magnitude of the decrease in $y_{O_2,CGO}$ after the setpoint changes are completed at $t_{end} = 26.25$ min is larger compared to $y_{O_2,GOX}$. By analogy to the GOX product, the slight decrease in $y_{O_2,CGO}$ during the setpoint changes can be explained using the S-factor S_{Ar} (see Figure 13). The significant drop of $y_{O_2,CGO}$ to a minimum of $y_{O_2,CGO,min} = 0.71$ at $t = 54.15$ min can be explained due to the composition changes of the liquid holdup in the sump of the CAC_1 (see Figure 12) over time.

Ar system

Now, the relevant response of the Ar system is presented. However, since the Ar system is highly dependent on the Ar column feed CGO, the graphs on the right side in Figure 11 are of additional importance here. Figure 12 shows the development of the bottom liquid molar fractions of O_2 x_{O_2,CAC_1} (top) and of Ar x_{Ar,CAC_1} (bottom) over time.

In the case of NLM, an increase in the molar fraction of Ar x_{Ar,CAC_1} at the expense of O_2 x_{O_2,CAC_1} can be observed. This is a result of the excess liquid holdup which accumulates in the column sumps. In the sump of the CAC_2, an Ar-rich liquid accumulates. The liquid
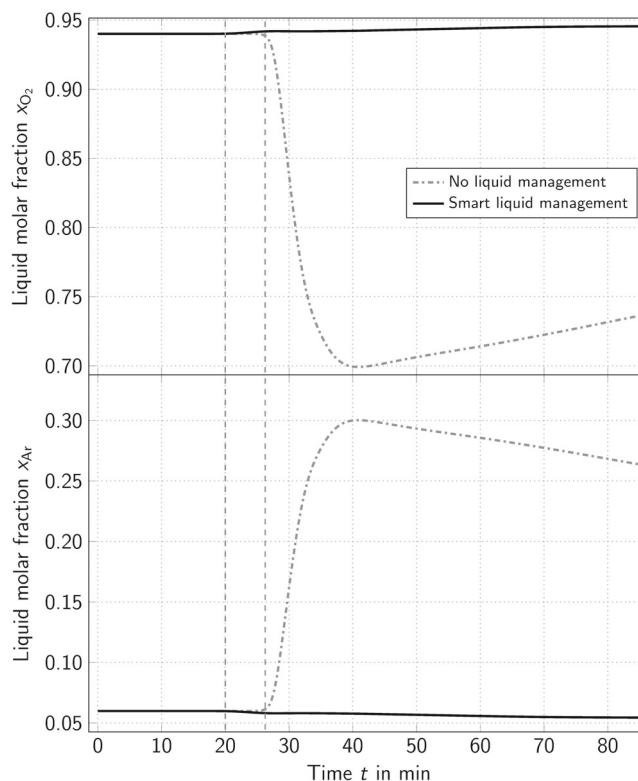

FIGURE 12 Plant response during the turn-down: Composition development of the liquid holdup in the sump of the CAC_1 over time. Liquid molar fraction of O_2 (top), liquid molar fraction of Ar (bottom)

holdup in the CAC_1 contains mainly O_2. The Ar-rich liquid from the CAC_2 is then fed to the CAC_1 causing an accumulation of Ar with a temporal delay. At $t \approx 54.17$ min, a maximum of the molar fraction of Ar $x_{Ar,CAC_1,max} = 0.289$ can be observed in the sump of the CAC_1. This liquid is then fed back to the LPC. Since the LPC feed stage of the reflux from the CAC_1 is identical to the withdrawal stage of the Ar column feed CGO, it impacts the CGO composition resulting in the graph of the O_2 vapor molar fraction $y_{O_2,CGO}$ at the upper right in Figure 11 after the end of the setpoint changes. However, the effect of the CACs sump liquid on $y_{O_2,CGO}$ is delayed in time compared to the impact of the internal flow condition changes in the LPC, which influence the composition of the Ar column feed CGO right after the start of the setpoint changes.

In the case of SLM, the Ar-rich liquid holdup is held back in the CAC_2 sump preventing the accumulation of Ar in the sump of the CAC_1 and, thus, preventing the reduction of the O_2 vapor molar fraction $y_{O_2,CGO}$. In addition, due to the specific manipulation of LPC fluid dynamics (see Figure 13), the O_2 vapor molar fraction $y_{O_2,GOX}$ of the GOX stream (see Figure 11, lower left) increases during the period of setpoint changes.

LPC fluid dynamics

Finally, the focus is on LPC fluid dynamics during the turn-down. Figure 13 shows the S-factor S_{Ar} of Ar at the first column tray of the LPC right above the MC (bottom) over time. The S-factor S_{Ar} is
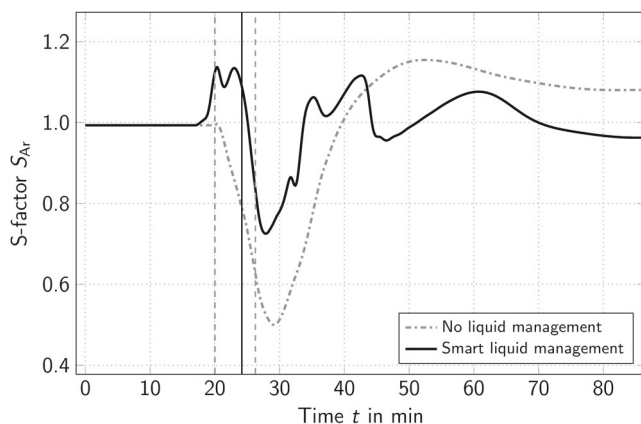
FIGURE 13 Plant response during the turn-down: S-factor of Ar S_{Ar} at the first column tray in the LPC above the MC

defined according to Equation (1). As this parameter strongly influences the GOX purity, there will be references to the lower left diagram of Figure 11.

Since the primary purpose of the column trays between the MC and the withdrawal of Ar column feed CGO is the separation of Ar and O_2, the S-factor of Ar is of particular interest. The initial value of S_{Ar} is slightly below one. That is, there is a separation between Ar and O_2 right above the MC. In detail, Ar is stripped downwards. With the beginning of the load change, in the case of NLM, the S-factor S_{Ar} decreases until it reaches a minimum at $t = 29.1$ min. The minimum value of the S-factor is $S_{Ar,min} = 0.5$, which is approximately the half of the initial value. Afterwards, the S-factor S_{Ar} eventually rises until, at $t = 39.75$ min, it reaches a value of $S_{Ar} \geq 1$.

The graph of the S-factor S_{Ar} can be used to explain the development of the O_2 vapor molar fraction $y_{O_2,GOX}$ over time, which is shown in the lower left diagram of Figure 11. Using NLM, the decrease in the O_2 molar fraction $y_{O_2,GOX}$ is evoked by $S_{Ar} < 1$ due to the fact that Ar is stripped towards the MC. With a delay of approximately 1.5 min after $S_{Ar} \geq 1$ (at $t = 39.75$ min), $y_{O_2,GOX}$ reaches its minimum and rises again due to the fact that with $S_{Ar} \geq 1$, Ar is increasingly rectified upwards.

As can be seen, the S-factor S_{Ar} is an early indication of the behavior of the GOX product purity $y_{O_2,GOX}$. Moreover, the S-factor S_{Ar} is used to derive the setpoint changes of the PC and CACs sump levels in previous simulation studies. To prevent the loss of GOX product purity $y_{O_2,GOX}$, the S-factor S_{Ar} can be manipulated accordingly. By applying SLM, that is, varying the liquid reflux to the LPC by adjusting the level setpoints of the PC and the CACs (see Figure 9), it is possible to increase the S-factor S_{Ar} before the setpoint changes start at $t_{start} = 20$ min evoking an increase in O_2 vapor molar fraction $y_{O_2,GOX}$ (see Figure 11, lower left). The liquid reflux to the LPC is manipulated in a way that the minimum of the S-factor is increased from $S_{Ar,min} = 0.499$ to $S_{Ar,min} = 0.725$ resulting in the adherence of the GOX product purity constraints. Afterwards the S-factor S_{Ar} oscillates around one with a small amplitude due to enduring changes of the internal column flows until it eventually converges to a value slightly below one.

To sum it up, the SLM is used to manipulate LPC fluid dynamics during the turn-down, which allows for the adherence to the GOX product purity $y_{O_2,GOX}$ during the whole load change procedure. Another aim of the SLM is to prevent the accumulation of Ar in the CAC_1 sump (see Figure 10) by accumulating the Ar-rich excess liquid holdup in the CAC_2, to prevent this liquid from being fed back to the LPC. The prolonging of the setpoint changes of the Ar system (see Figure 8, right side) is an additional measure to increase the GOX product purity $y_{O_2,GOX}$ during the load change procedure by temporarily removing the intermediate boiling component Ar from the LPC disproportionately. However, the influence of this deceleration is comparatively small.

The magnitude, start time and duration of the setpoint changes shown in Figure 9 are derived from additional simulation studies using the S-factor S_{Ar} as indicator (see Figure 13), which is explained in Section 4. However, a constraint for the level setpoint changes is, for instance, the impact on the MC level (see Figure 11, upper right). Here, the early start times of the setpoint changes of the PC and CAC levels result in a decrease in the MC level L_{MC} before the turn-down starts at $t = 20$ min. This decrease needs to be minimized. Further constraints are the actual sump geometries, which limit the maximum liquid level of the corresponding column.

Eventually, the power consumptions of both cases are compared as an indication of the operational expenses (OPEX). The main contributors to the ASU's energy balance are the main air compressor and the turbine. Since the graphs of the main air flows (see Figure 8, upper left) of SLM and NLM are identical, the MAC power consumptions are identical as well. Compared to the energy intake of the main air compressor, the contribution of the turbine is marginal. Thus, the OPEX of both concepts is equal.

This study outlines the importance and benefits of applying a DT of an ASU to improve plant operations. Due to the abundance of data, the DT provides a highly detailed insight into transient plant behavior during load change procedures. It is of particular importance to analyze non-feasible load changes, that is, violating purity constraints, in offline studies. This allows for the identification of bottlenecks and the development of operational concepts such as SLM and, thus, faster load change procedures. The SLM concept is in accordance with the experience of plant operators and automation engineers to accelerate load change procedures of ASUs at Linde. However, these results are in contrast with the findings of Cao et al.[42] as they claim that a preemptive control action tend to result in plant closer to its boundaries. In this study, the preemptive action of SLM is required to successfully conduct this load change procedure without violating any purity constraint, that is, to increase the load change rate of the ASU. An additional benefit of the DT is that it allows quantification and visualization of the effects of operating strategies on plant operation during load change procedures. Furthermore, by means of dynamic simulation, the DT enables an in-depth analysis and optimization of existing operating concepts, which are based on many years of experience. In addition, non-measurable quantities such as the S-factor S_{Ar} are identified as key parameters to improve the presented turn-down, emphasizing the importance of a

DT of the ASU or only of the LPC as a soft sensor for (flexible) plant operations.

5.2 | Turn-up

During a fast turn-up, the main challenges are to compensate for a temporary lack of liquid holdup on each column tray and the adherence to the purity constraints for the low boiling components (see Table 2). Both challenges are a result of an increase in the reboil ratio in all columns during the load change. This is a result of a rapid increase in the main air flow $\dot{V}_{Air}$ coupled to an increased MC heat duty $\dot{Q}_{MC}$. Due to the higher amount of vapor flow, more liquid holdup is required on each column tray to overcome the increased flow resistance. Thus, the liquid flow to the corresponding column sumps is slowed down, which leads to a level decrease in the corresponding column sumps and the MC level L_{MC}. This is challenging for two reasons. First, a decrease in MC level L_{MC} impacts the duty $\dot{Q}_{MC}$ and second, the MC needs to be covered in liquid to a certain extent at all times for safety reasons. The decelerated liquid flow can be observed in all columns.

Conversely, this means that during a turn-up fluid dynamics in the LPC promote the high boiling component O_2 in the GOX product. The separation of Ar between the withdrawal of CGO and the MC is enhanced since a decrease in the liquid flow increases the S-factor (see Equation 1). Here, the idea of SLM is to temporarily enhance the liquid flow to the LPC at the expense of GOX purity $y_{O_2,GOX}$ without violating any constraints. Thus, on the one hand, a major drop in the MC level L_{MC} can be prevented. On the other hand, the adherence to the low boiler purities can be achieved. This can be accomplished by using the excess liquid, which is buffered in the PC and CAC sumps during the turn-down.

In the case of SLM, the level setpoints of the PC and the CAC are adjusted in start time and duration with regard to the remaining load change. Furthermore, the setpoint changes for the Ar system as well as the LIN reflux to the LPC are prolonged using SLM. In the case of NLM, all controller setpoints for composition, flow and pressure control (see Figure 3 for the control loops) are ramped up linearly to their full load values. The level setpoints for all condenser/reboilers remain constant at 100% to keep the condenser blocks covered in liquid at all time. In addition, the remaining level setpoints for the column sumps of the PC and both the CACs also remain at their initial value.

For the analysis of the turn-up scenario, a time period of 250 min is considered. Starting at the final steady-state of the turn-down with SLM at 50% load, the turn-up starts at $t_{start} = 20$ min and ends at $t_{end} = 26.25$ min. The total duration is $\Delta t = 6.25$ min. The required setpoints for the load change can be taken from steady-state operation at 100% load, which is equal to the initial state of the turn-down and the setpoint changes are linear in nature.

Although not all relevant parameters have reached their final part-load values at $t = 250$ min, this time span is sufficient to describe all
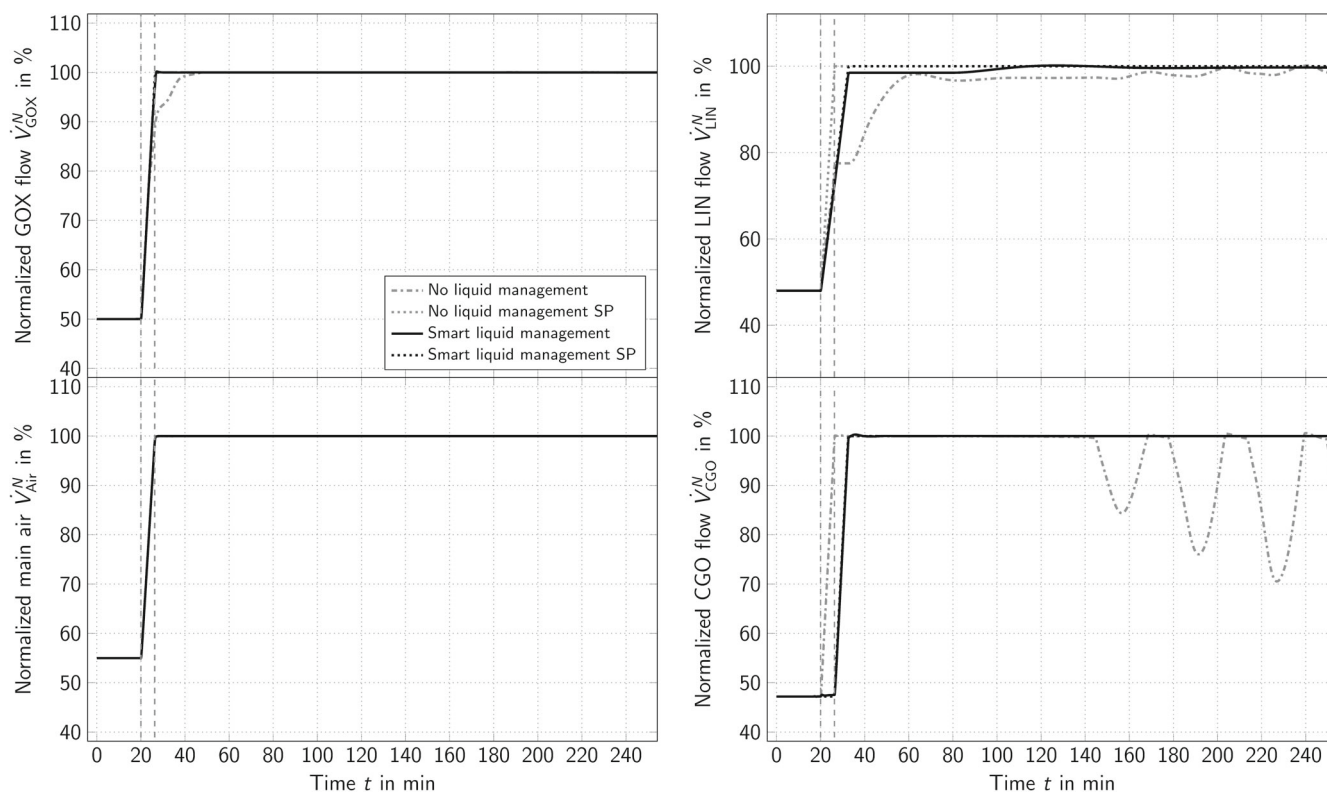

FIGURE 14 Controller inputs for the turn-up: normalized GOX flow (upper left), normalized air flow (lower left), normalized LIN flow (upper right) and normalized CGO flow (lower right)

relevant aspects of the plant response during the turn-up. In some cases, the final steady-state is obtained after several days, for instance the purity of the GOX product in the case of NLM. By analogy to the turn-up scenario, a successful load change does not require all concentrations to reach steady-state as long as the changes are minor and the purity constrains are met. The required CPU time for the simulation using SLM is approximately 1 h and 15 min on the used workstation. The NLM case required a CPU time of approximately 11 h due to the N_2 breakthrough, which is explained later in Section 5.2.2. The relevant setpoint changes for the turn-up are presented in Section 5.2.1. The plant response and the impact of SLM are discussed in Section 5.2.2.

5.2.1 | Controller inputs

This section presents the relevant controller inputs for the analysis of the turn-up. In contrast to the turn-down, noticeable deviations between the setpoint changes and the controlled variables occur during the turn-up due to a N_2 breakthrough, which is explained in detail in Section 5.2.2. The N_2 breakthrough affects the whole plant emphasizing the high degree of heat and process integration of an ASU with Ar separation.

Figure 14 shows the setpoint changes of the turn-up for the GOX product $\dot{V}_{GOX}$ (upper left), the main air $\dot{V}_{Air}$ (lower left), the LIN $\dot{V}_{LIN}$ (upper right), and the Ar column feed CGO flow $\dot{V}_{CGO}$ (lower right). The CGAR flow change is not shown here as the duration and shape

of the CGAR and CGO setpoint changes are identical. In addition, the start and end times of the load change are marked with vertical gray dotted lines in all of the following figures.

By analogy to the turn-down, in the case of NLM, all setpoint changes for the turn-up start and end at the same time. However, apart from the main air flow $\dot{V}_{Air}$ (lower left), the graphs of the controlled variables differ from the setpoints. As for the LIN reflux $\dot{V}_{LIN}$ to the LPC (see Figure 14, upper right), the course of the actual LIN flow can be explained by the type of control used (see Figure 3). Here, a trim control configuration is used. That is, the manual output of the AC is changed during the turn-up (feedforward) but the controller is allowed to correct its output in a specific range ($\varepsilon_{Trim,AC} = 22.5\%$) around the manual output (feedback) to fulfill its task. This results in the deviation of actual LIN reflux and the setpoint. In the case of SLM, the deviations of setpoint and controlled variable are marginal. In addition, the setpoint change for the LIN reflux $\dot{V}_{LIN}$ to the LPC is prolonged ending at $t = 32.5$ min with a duration of $\Delta t = 12.5$ min.

By using SLM, the setpoint change for the Ar system (see Figure 14, lower right) is shifted in time. It starts at $t = 26.25$ min and ends at $t = 32.5$ min. However, the duration of the setpoint changes remains $\Delta t = 6.25$ min. Further, no deviations between setpoint and controlled variable can be observed.

In the case of NLM, an oscillating behavior of the actual CGO flow $\dot{V}_{CGO}$ around its setpoint starting at $t \approx 145$ min can be seen, which is a result of the N_2 breakthrough. This term refers to the vapor molar fraction $y_{N_2,CGO}$ of the Ar column feed CGO. If $y_{N_2,CGO}$
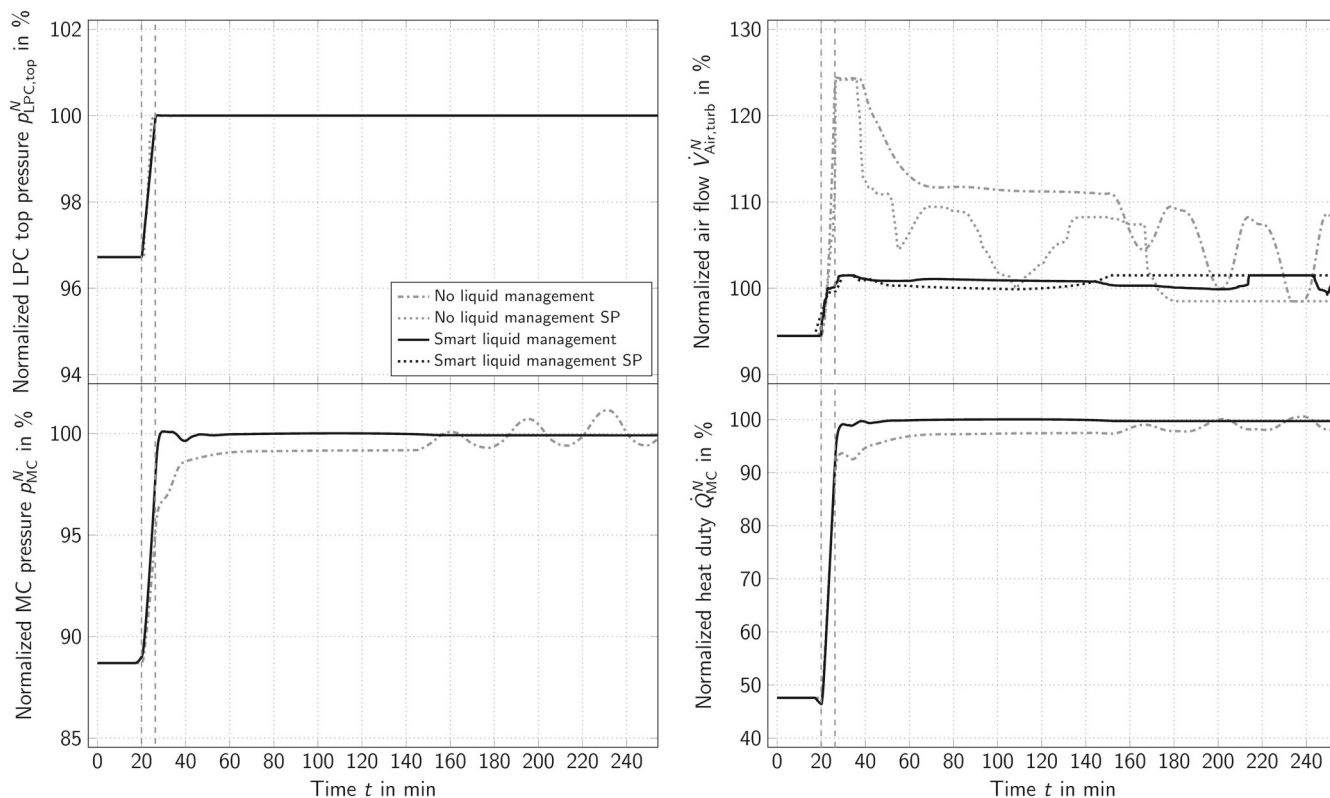

FIGURE 15 Controller inputs for the turn-up: LPC top pressure (upper left) and normalized turbine air flow (upper right), plant response for the normalized MC pressure (lower left) and normalized MC heat duty (lower left)

rises above a critical threshold, and starts to influence the crude Ar condenser/reboiler duty $\dot{Q}_{\text{cond/reb,CAC}}$ and, thus, the CAC fluid dynamics, the term N_2 breakthrough is used. In general, this circumstance causes oscillations of most of the considered parameters in the case of NLM.

Using NLM, the behavior of the GOX product flow $\dot{V}_{\text{GOX}}$ between $t \approx 23.33$ min and $t \approx 41.67$ min is a result of the size of the GOX product valve and the increased turbine flow (see Figure 15, upper right) which is required due to the MC level control. The increased turbine flow $\dot{V}_{\text{Air,turb}}$ has a major impact on the further course of the entire turn-up, which is discussed below.

Figure 15 shows the setpoint changes of the LPC top pressure $p_{\text{LPC,top}}$ (upper left) as well as the turbine flow $\dot{V}_{\text{Air,turb}}$ resulting from the MC level control (upper right) and the plant response for the MC pressure p_{MC} (lower left) and the MC duty $\dot{Q}_{\text{MC}}$ (lower right) for both cases. The graphs of these values are required to explain the deviations between setpoint and controlled variable in the case of NLM, illustrated in Figure 14.

By analogy to the control scheme of the LIN reflux to the LPC, a trim control configuration is used for the MC level control (turbine flow). In the NLM case, a larger range for possible corrections of the turbine flow is required due to the massive lack of liquid holdup in the MC (see Figure 18, upper left). This explains the different upper boundaries for the turbine flow of $\dot{V}_{\text{Air,turb,ub}} = 124.4\%$ (NLM) and $\dot{V}_{\text{Air,turb,ub}} = 101.5\%$ (SLM). A decrease in MC level L_{MC} requires additional refrigeration duty (cryogenic liquid make-up).

However, the total amount of air $\dot{V}_{\text{Air}}$ is equal in both cases. This results in different amounts of air fed to the PC, which leads to different MC duties $\dot{Q}_{\text{MC}}$ (lower right) causing different fluid dynamic conditions in the LPC. Thus, a higher turbine flow results in a higher gas load in the upper part of the LPC but a lower gas load in the part below the turbine feed tray. This leads to the effect that, although the setpoint changes for the LPC top pressure are identical in both cases, the course of the MC pressure p_{MC} differs. In the case of NLM, the MC pressure levels are below the SLM pressure levels until $t \approx 145$ min. Afterwards, using NLM, p_{MC} starts oscillating around the constant course of p_{MC} using SLM. In addition, the pressure increase in the MC is slower in the NLM case compared to SLM. The more inert behavior of $\dot{V}_{\text{GOX}}$ using NLM (see Figure 14, upper left) is a result of the slower increase in the MC pressure p_{MC} although the GOX product valve is opened completely.

Figure 16 shows the levels L_{PC}, $L_{\text{CAC,1}}$, and $L_{\text{CAC,2}}$ and their setpoint changes for the PC and both CACs.

By analogy to the turn-down scenarios, all level setpoint changes start prior to the actual load change at $t = 16.875$ min. Here, all three setpoint changes end at a different time. The setpoint change for the PC ends at $t = 26.25$ min, for the CAC_1 at $t = 32.5$ min, and the CAC_2 at $t = 38.75$ min. In addition, it is very noticeable that the end values of the level setpoint changes for the PC $L_{\text{PC,end}} = 118\%$ and for the CAC_2 $L_{\text{CAC2,end}} = 88\%$ differ from the initial state (100%). Thus, the level setpoint changes of the turn-down
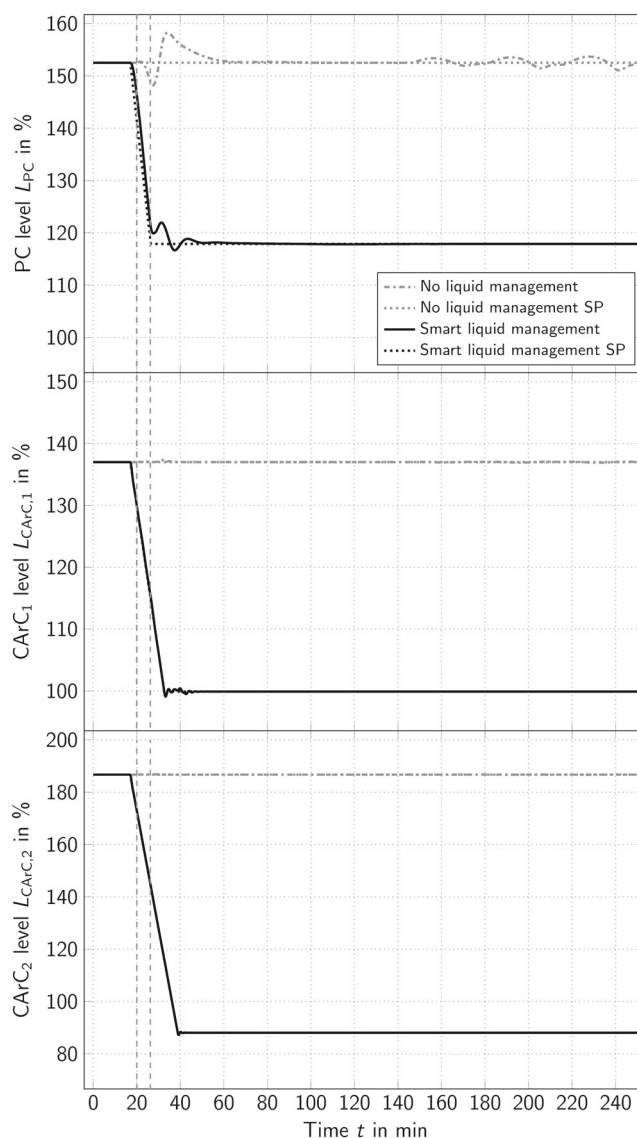

FIGURE 16 Controller inputs for the turn-up: PC sump level (top), CAC_1 sump level (middle) and CAC_2 sump level (bottom)

and turn-up are non-symmetrical. Despite this being interesting and requiring further investigation, it is not subject of this work, considering the length of the article.

5.2.2 | Plant response

In the following, the plant response during the turn-up is presented. First, the behavior of the low boiling components N_2 at the top of the PC and the LPC as well as Ar at the top of the CAC is discussed. Then, the focus is on the lower part of the LPC including the Ar column feed CGO and the high boiler GOX in the MC. Afterwards, the response of the Ar system is presented with regard to the N_2 breakthrough. Finally, LPC fluid dynamics are discussed in detail.

Low boiling components

A major challenge of the turn-up is to preserve the purity requirements for the low boiling components in the GAN, PGAN and CGAR streams due to an increased vapor flow through the columns and the resulting deceleration of liquid flow. Figure 17 shows the O_2 vapor molar fractions $y_{O_2,GAN}$, $y_{O_2,PGAN}$, and $y_{O_2,CGAR}$ of the GAN, PGAN, and CGAR streams over time.

In the case of NLM, the purity constraints of GAN and CGAR are violated during the load change. However, the purity constraint of the PGAN stream is met during the entire load change with only minimal deviations from its initial value. In the case of SLM, only the purity constraint of the GAN stream is minimally violated for a short period of time. The graphs of the GAN and PGAN purities $y_{O_2,GAN}$ and $y_{O_2,PGAN}$ are a result of the behavior of the LIN reflux $\dot{V}_{LIN}$ (see
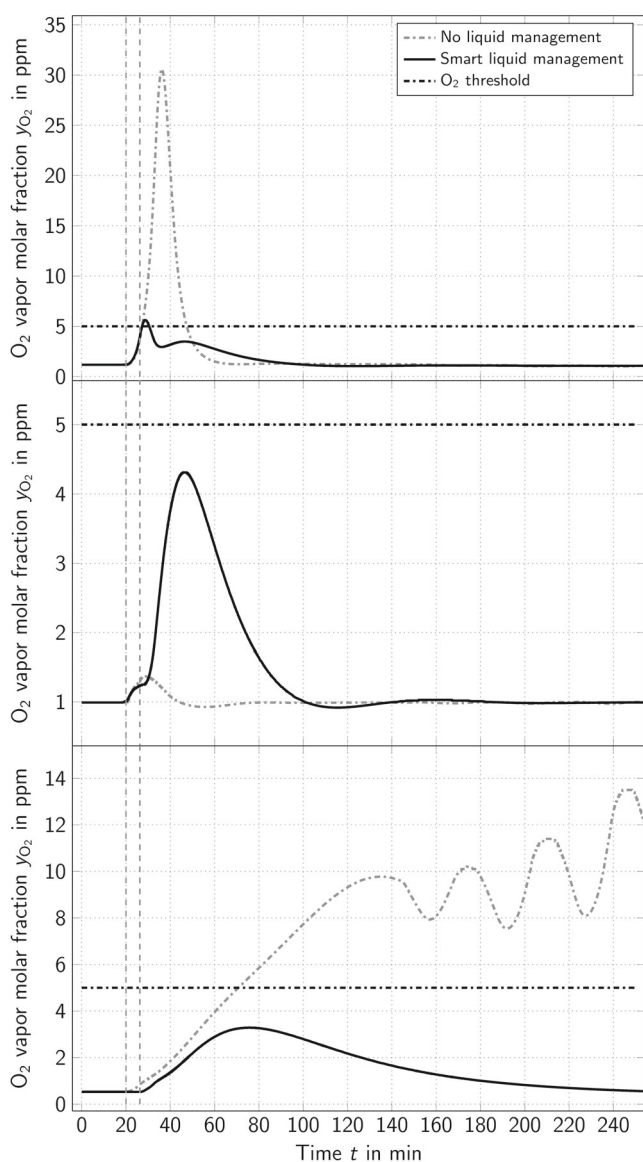
Figure 14, upper right) over time. In the case of NLM, the LIN reflux $\dot{V}_{LIN}$ increases more slowly compared to the SLM case resulting in a higher PGAN purity due to increased reflux to the PC. However, the high PGAN purity $y_{O_2,PGAN}$ in case of NLM comes at the expense of the GAN purity $y_{O_2,GAN}$, which can be seen at the top of Figure 17. In the case of SLM, the deceleration of the LIN reflux setpoint change leads to a more equal distribution of LIN to either the PC or the LPC. Thus, both purity constraints $y_{O_2,PGAN}$ and $y_{O_2,GAN}$ can be met apart from the minimal violation of the GAN purity starting at $t = 27.28$ min until $t = 30.52$ min with a maximum of $y_{O_2,GAN,max} = 5.61$ ppm. Here, a bottleneck for the load change rate is identified, which cannot be solved by the presented operational strategy (SLM). This requires a potential structural measure at the plant, for instance, an additional LIN buffer vessel between the PC and the LPC.

Regarding CGAR purity $y_{O_2,CGAR}$, in the case of NLM, the purity constraint is violated at $t = 70.25$ min and the graph oscillates as a result of the N_2 breakthrough starting at $t \approx 145$ min. In the case of SLM, the CGAR purity constraint can be met during the entire load change procedure. The delay of the setpoint changes of the Ar system (see Figure 14, lower left) is an additional measure to keep the O_2 molar fraction of the CGAR stream $y_{O_2,CGAR} \leq 5$ ppm.

LPC—lower part

Figure 18 illustrates the plant response regarding the MC level L_{MC} (top) and the O_2 vapor molar fraction $y_{O_2,GOX}$ of the GOX product (bottom) on the left side, whereas the Ar column feed CGO vapor molar fractions ($y_{O_2,CGO}$ at the top and $y_{N_2,CGO}$ at the bottom) are shown on the right side.

The graph on the upper left side of Figure 18 illustrates the impact of the fast increase in the reboil ratio in the LPC and the resulting decelerated liquid flow to the columns sumps. In case of NLM, the MC level L_{MC} decreases rapidly with the beginning of the turn-up at $t_{start} = 20$ min until it reaches its minimum $L_{MC,min} = 60.3\%$ at $t = 37.55$ min. Afterwards, it starts to converge to its initial value slowly. The significant decrease in the MC level L_{MC} requires an increased amount of turbine flow $\dot{V}_{Air,turb}$ (see Figure 15, upper right), which eventually causes the N_2 breakthrough. By analogy to all the remaining values affected by the N_2 breakthrough, the MC level L_{MC} starts oscillating at $t \approx 145$ min. Furthermore, the decrease in MC level would be intolerable in real plant operations emphasizing the importance of an in silico investigation of this procedure using the DT. With SLM, the MC level L_{MC} increases at first, as the level setpoint changes start prior to the remaining load change (see Figure 16). The variation of the MC level L_{MC} is reduced to a range of ±7%.

The graph of the O_2 vapor fraction $y_{O_2,GOX}$ of the GOX product is shown in the lower left diagram in Figure 18. As can be seen, using NLM, the O_2 vapor molar fraction of the GOX product $y_{O_2,GOX}$ starts to increase with the beginning of the turn-up until it reaches its maximum $y_{O_2,GOX,max} = 0.9985$ at $t = 54.25$ min. Afterwards, it starts to decrease due to the increased turbine flow $\dot{V}_{Air,turb}$ (see Figure 15, upper right). At $t \approx 145$ min, an oscillating behavior can be observed resulting in a violation of the purity constraint of 0.995 at $t = 159.93$ min. With the MC level L_{MC} reaching the desired value of

FIGURE 17 Plant response during the turn-up: O_2 vapor molar fraction of the top products of the distillation columns. LPC-GAN (top), PC-PGAN (middle) and CAC-CGAR (bottom)

$L_{MC} = 100\%$, the required turbine flow $\dot{V}_{Air,turb}$ decreases. Eventually, this leads to a convergence of $y_{O_2,GOX}$ with its desired value. As this takes ≈ 1.75 d it is not visualized.

With SLM, the purity constraint for the GOX product is met at all times. Nevertheless, the graph of $y_{O_2,GOX}$ decreases, starting at the $t = 16.875$ min. At the expense of GOX purity $y_{O_2,GOX}$, a rapid decrease in the MC level L_{MC} is prevented. By analogy to the turn-down, the S-factor S_{Ar} shown in Figure 20 can be used as an indication to find a feasible trade-off between $y_{O_2,GOX}$ and L_{MC} using the liquid in the PC and CAC sumps for SLM. At a simulated time of $t \approx 150$ min, the graph of $y_{O_2,GOX}$ decreases again as a result of the turbine flow $\dot{V}_{Air,turb}$ (see Figure 15, upper right), which is also slightly above its desired value of 100% until the MC level eventually reaches its target value of $L_{MC} = 100\%$. However, the purity constraint of $y_{O_2,GOX} \geq 0.995$ is met at all times. During the turn-up, one aim of the SLM concept is to find the maximum possible amount of liquid, which can be fed from the remaining columns to the MC, without violating the purity constraint of $y_{O_2,GOX} \geq 0.995$ and while preventing a significant decrease in MC level L_{MC}. This helps to avoid a N_2 breakthrough caused by an increased turbine flow $\dot{V}_{Air,turb}$ over a long period of time.

The graph of the O_2 vapor molar fraction $y_{O_2,CGO}$ of the Ar column feed CGO (upper right) is similar to the graph of the O_2 vapor fraction of the GOX product $y_{O_2,GOX}$ in both cases. By analogy to the turn-down, a small excerpt is shown in this diagram, which illustrates the course of $y_{O_2,CGO}$ over 3300 min. It shows that by using SLM, a constant graph is reached at $t \approx 250$ min. For the NLM case, it is shown that at $t \approx 1400$ min $= 1$ d the oscillations have stopped and the O_2 vapor fraction of the CGO stream has already recovered. At $t \approx 2520$ min $= 1.75$ d, $y_{O_2,CGO}$ converges to the value of the SLM case. In the case of NLM, a maximum of $y_{O_2,CGO,max} = 0.962$ can be observed at $t = 32.2$ min. After that, a short decrease occurs and flattens at $t \approx 41.27$ min. At $t = 145$ min an oscillating behavior can be detected due to the N_2 breakthrough. The fast decrease in $y_{O_2,CGO}$ is a result of the fast increase in the LPC's reboil ratio. In case of SLM, a slight overall decrease in $y_{O_2,CGO}$ can be observed due to the different O_2 vapor fractions of the CGAR stream $y_{O_2,CGAR,50\%} = 0.53$ ppm in part-load operation and at the initial operating point of 100% load $y_{O_2,CGAR,100\%} = 0.717$ ppm. The larger the amount of O_2 in the CGAR stream, the lower the O_2 vapor molar fraction $y_{O_2,CGO}$.

At the lower right of Figure 18, the graph of the N_2 vapor molar fraction $y_{N_2,CGO}$ is shown. In case of SLM, there is only a slight increase in N_2 in the Ar column feed CGO with a maximum of $y_{N_2,CGO,max} = 6.1 \times 10^{-4}$ at $t = 23.62$ min. For the considered turn-up, this vapor molar fraction of N_2 $y_{N_2,CGO}$ is tolerable as it does not influence the crude Ar condenser/reboiler duty $\dot{Q}_{cond/reb,CAC}$ (see Figure 19, bottom). In case of NLM, the N_2 breakthrough can be observed as the vapor molar fraction of N_2 $y_{N_2,CGO}$ starts to affect the crude Ar condenser/reboiler duty $\dot{Q}_{cond/reb,CAC}$ (see Figure 19, bottom) and, thus, the overall plant.
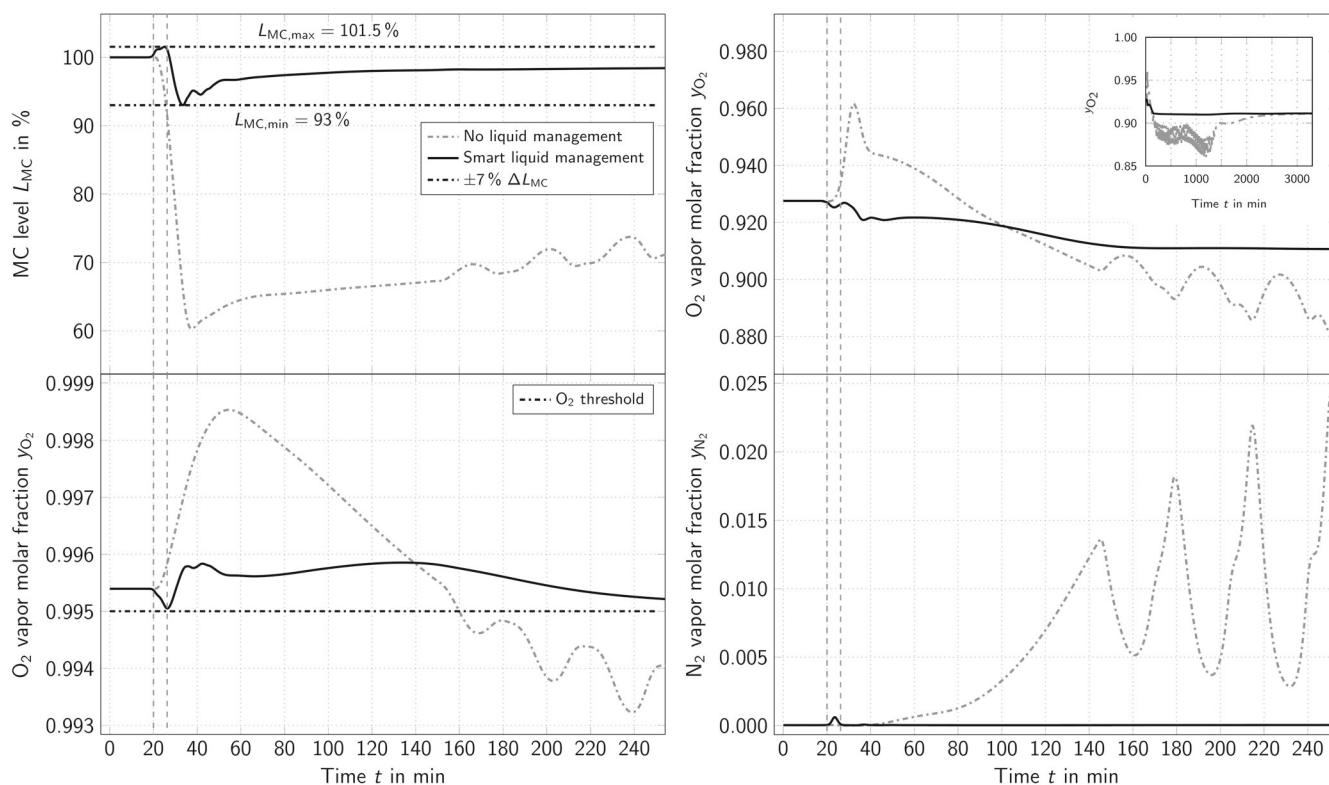

FIGURE 18 Plant response during the turn-up: MC level (upper left), O_2 molar fraction of the GOX product (lower left), O_2 molar fraction of the Ar column feed CGO (upper right), N_2 molar fraction of the Ar column feed CGO (lower right)

Ar system

The oscillating behavior as a consequence of the N_2 breakthrough can be explained using the N_2 vapor molar fraction of the crude Ar product CGAR $y_{N_2,CGAR}$ (top) and the crude Ar condenser/reboiler duty $\dot{Q}_{cond/reb,CAC}$ (bottom), which are shown in Figure 19. These graphs are a result of the N_2 vapor molar fraction in the Ar column feed CGO $y_{N_2,CGO}$.

Using NLM, the first maximum of $y_{N_2,CGO,max}$ can be seen at $t \approx 145.83$ min (see Figure 18, lower right). There is a time delay of
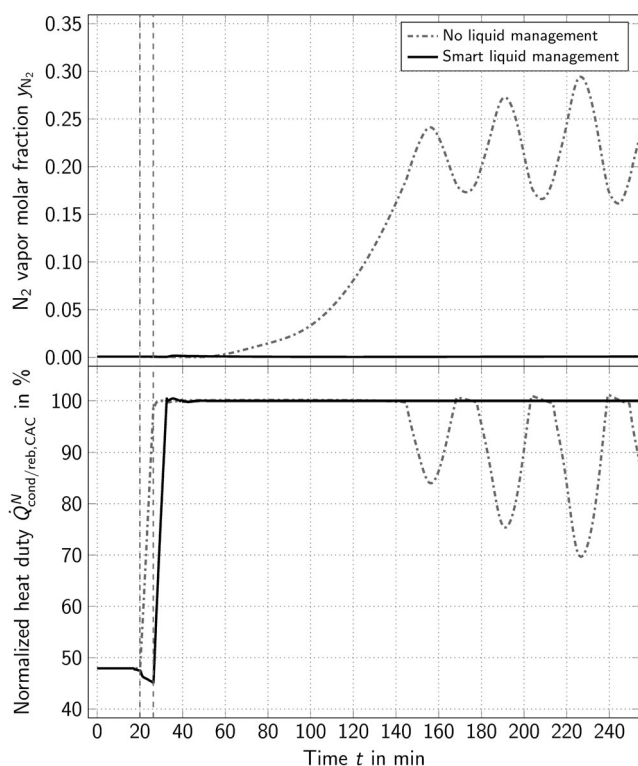

FIGURE 19 Plant response during the turn-up: N_2 vapor molar fraction of the CGAR stream (top), normalized crude Ar condenser/reboiler duty (bottom)
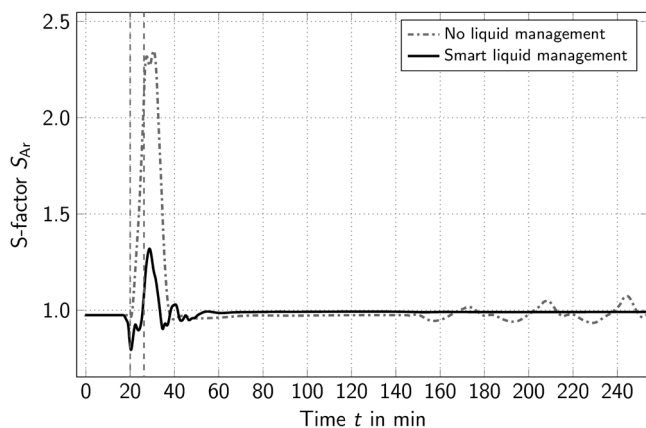

FIGURE 20 Plant response during the turn-up: S-factor of Ar S_{Ar} (bottom) at the first column tray in the LPC above the MC

$\Delta t \approx 12.2$ min until the N_2 is propagated to the top of the CAC due to the vapor holdup and equilibrium changes inside the column. This leads to the first maximum of $y_{N_2,CGAR,max}$ at $t \approx 164.03$ min. Above the critical amount of $y_{N_2,CGAR,crit} \approx 0.16$, a further increase in N_2 leads to a subsequent decrease in the crude Ar condenser/reboiler duty $\dot{Q}_{cond/reb,CAC}$ since the amount of N_2 significantly influences the dew temperature of the CGAR $T_{Dew,CGAR}$. This leads to a decrease in liquid reflux for the CAC and consequently reduces the amount of Ar column feed CGO, which is withdrawn from the LPC. However, since the amount of CGO is subject to flow control, the pressure on the reboiler side of the crude Ar condenser/reboiler is adjusted to re-establish the required duty $\dot{Q}_{cond/reb,CAC}$. Thus, the amount of liquid reflux is varied to achieve the correct pressure resistance for the CGO feed to match its setpoint (see Figure 14, upper right). However, the temporary decrease in liquid reflux for the CAC impacts the entire plant. Since the CAC liquid reflux is finally fed back to the LPC, it eventually has an effect on the LPC's fluid dynamics and the MC. Thus, with a temporary lower liquid flow from the CAC to the LPC, the MC level L_{MC} (see Figure 18, upper left) and subsequently the MC duty $\dot{Q}_{MC}$ (see Figure 15, lower right) decrease. In addition, the GOX product purity $y_{O_2,GOX}$ (see Figure 18, lower left) is influenced due to the development of the MC duty $\dot{Q}_{MC}$ over time. This eventually feeds back to the composition at the Ar column feed CGO, which causes the oscillations.

Since the MC level L_{MC} (see Figure 18, upper left) increases slowly, the turbine flow $\dot{V}_{Air,turb}$ converges to its nominal value of 100%. The final value is reached at $t \approx 1$ d, steadily increasing the LPCs reboil ratio and the GOX product purity $y_{O_2,GOX}$ during the level build-up. This leads to a decrease in the N_2 vapor molar fraction $y_{N_2,CGO}$ at the Ar column feed CGO below the critical amount. Thus, the crude Ar condenser/reboiler duty $\dot{Q}_{cond/reb,CAC}$ is not affected anymore. In other words, without SLM, the plant would suffer a product loss for a period of $t \approx 1$ d. However, with manual interventions into plant control, it might be possible to reduce the downtime. But a N_2 breakthrough always results in the loss of value products, which needs to be prevented at all times.

LPC fluid dynamics

Figure 20 shows the S-factor of Ar S_{Ar} at the first column tray right above the MC over time.

In the case of NLM, S_{Ar} is more than doubled, leading to the increase in GOX product purity $y_{O_2,GOX}$ at the expense of MC level L_{MC} (see Figure 18, left side). In case of SLM, the level setpoint changes of the PC and CAC (see Figure 16) lead to a reduction in the amplitude of the S-factor S_{Ar} during the entire turn-up. Also, since setpoint changes of the levels start prior to the remaining load change, an initial decrease in the S-factor S_{Ar} can be observed. As already elaborated, the primary target of SLM is to prevent the decrease in MC level L_{MC} at the expense of GOX product purity $y_{O_2,GOX}$ without violating the corresponding purity constraints. This can be achieved by keeping the course of S_{Ar} relatively constant.

However, the SLM for the turn-up requires excess liquid in the plant. Therefore, it must be ensured in a previous turn-down that

enough liquid is collected in the respective sumps. In addition, after the turn-up with SLM has been completed, an equalization process is required to restore the column sump levels to their initial values. Otherwise, rapid load change sequences can lead to problems in liquid management. By analogy to the turn-down, the power consumptions of the NLM and SLM are compared as an indication of the OPEX, which is also equal for both cases.

This case study emphasizes the necessity for DTs to a priori analyze load change procedures. It is now possible to obtain valuable insight into scenarios, which are to be avoided when operating a real plant. Hence, no plant data is available and virtual studies are the only options of investigation. Being able to simulate the NLM case allows for the analysis and debottlenecking of the turn-up procedure without the consequences of $t \approx 1$ d product loss. In addition, it is possible to investigate upset scenarios such as the N_2 breakthrough in order to derive measures to prevent it or develop strategies to reduce downtime afterwards.

6 | CONCLUSION

In this work, the concept of a DT for ASUs introduced in Kender et al.[1] is applied to an industrially relevant ASU with Ar separation, emphasizing the increased complexity of this ASU topology. Apart from the additional equipment requirements, the separation of Ar also increases the degree of heat and process integration as well as the complexity of the control scheme. This is challenging for (in silico) plant operations, the simulation models and the used numerical solution algorithms. The presented case studies are challenging load change procedures in terms of agility and range. A turn-down and a turn-up from 50% to 100% and vice versa with a load change rate of 8% min^{-1} are simulated. Two operational concepts are compared, NLM and SLM. The main difference between the two concepts is the management of either the temporary excess (turn-down) or lack (turn-up) of liquid holdups in the different distillation columns. Using SLM, during the turn-down, the additional liquid holdup is buffered in the sumps of the PC and the CACs. The buffered liquid can then be used to supply the MC with the additional liquid required during the turn-up. Additional offline studies can be used to further optimize the magnitude, duration and start time of the respective level setpoint changes. The SLM concept allows for the performance of these load changes without the adherence to purity constraints. In addition, the in silico analysis of load changes using NLM, which entails a product loss as a consequence, reveals information regarding bottlenecks for rapid load change procedures, helps to identify new key parameters for an advanced plant operation evaluation (S-factor) or enables the investigation of upset scenarios (N_2 breakthrough), which have to be avoided during real plant operation. However, the derived setpoint changes using SLM are plant specific. These analyses can be carried out for the different ASU topologies and used as a starting point for individual adaptation of setpoint changes on-site to allow for faster load changes at real plants.

Furthermore, being able to monitor column fluid dynamics (S-factor) in real time is an enormous benefit for plant operations as it can be used as an early indication of the change of product purities.

Thus, additional work should be put into further developing of the DT toward real-time capability to be able to use it as a soft sensor for the entire plant, or at least for stand-alone unit operations, such as the LPC. Real-time capability of the DT is a first step toward dynamic optimization, which potentially allows to further increase the load flexibility of an ASU, exceeding the presented linear load change procedures. In addition, the abundance of data generated by the DT allows for a better formulation of the dynamic optimization problem including the consideration of variables such as the S-factor.

CONFLICT OF INTEREST

The authors declare no potential conflict of interests.

AUTHOR CONTRIBUTIONS

Robert Kender: Conceptualization (lead); formal analysis (lead); investigation (lead); methodology (lead); validation (lead); writing – original draft (lead). **Felix Rößler:** Conceptualization (supporting); methodology (supporting); validation (supporting); writing – review and editing (lead). **Bernd Wunderlich:** Conceptualization (supporting); investigation (supporting); methodology (supporting); project administration (equal); software (equal); validation (supporting); writing – review and editing (equal). **Martin Pottmann:** Conceptualization (supporting); investigation (supporting); validation (supporting); writing – review and editing (equal). **Ingo Thomas:** Methodology (supporting); software (equal); writing – review and editing (supporting). **Anna-Maria Ecker:** Project administration (equal); validation (supporting); writing – review and editing (supporting). **Sebastian Rehfeldt:** Funding acquisition (lead); project administration (equal); validation (supporting); writing – review and editing (equal). **Harald Klein:** Resources (lead); supervision (lead); validation (supporting); writing – review and editing (supporting).

DATA AVAILABILITY STATEMENT

The data that support the findings of this study are available from Linde Engineering. Restrictions apply to the availability of these data, which were used under license for this study. Data are available from the corresponding author with the permission of Linde Engineering.

NOTATION

Symbols

h_P	packing height (m^3)
h_v	valve stroke (%)
K_i	vapor–liquid equilibrium ratio of component i (mol/mol)
$\dot{L}/\dot{G}$	ratio of liquid to gas flows (-)
L	liquid level (%)
n	tray number ($-$)

p	pressure (MPa)
$\dot{Q}$	heat duty (MW)
t	time (min)
T	temperature (K)
V	volume (m^3)
$\dot{V}$	volume flow (m^3/s)
x_i	liquid molar fraction (-)
y_i	vapor molar fraction (-)
z_i	bulk molar fraction (-)
δ	deviation (%)
Δp	pressure difference (MPa)
Δt	period of time (min)
ε_{Trim}	trim control range (%)

Subscripts

100%	regarding 100% plant load
50%	regarding 50% plant load
boil	boiling point
bub	bubble point
cond/reb	condenser/reboiler
crit	critical
dew	dew point
max	maximal
min	minimal
ub	upper bound

Superscripts

N	normalized

ORCID

Robert Kender https://orcid.org/0000-0001-5389-0383

REFERENCES

1. Kender R, Kaufmann F, Rößler F, et al. Development of a digital twin for a flexible air separation unit using a pressure-driven simulation approach. *Comput Chem Eng*. 2021;151:107349.
2. Haider P, Freko P, Acher T, Rehfeldt S, Klein H. A transient three-dimensional model for thermo-fluid simulation of cryogenic plate-fin heat exchangers. *Appl Therm Eng*. 2020;180:115791.
3. Kender R, Wunderlich B, Thomas I, Peschel A, Rehfeldt S, Klein H. Pressure-driven dynamic simulation of distillation columns in air separation units. *Chem Eng Trans*. 2018;69:271-276.
4. Kender R, Wunderlich B, Thomas I, Peschel A, Rehfeldt S, Klein H. Pressure-driven dynamic simulation of start up and shutdown procedures of distillation columns in air separation units. *Chem Eng Res Des*. 2019;147:98-112.
5. Klein H, Fritsch P, Haider P, et al. Flexibler Betrieb von Luftzerlegungsanlagen. *Chem Ing Tech*. 2020;92(12):1921-1940.
6. Fritsch P, Hoffmann R, Flüggen R, Haider P, Rehfeldt S, Klein H. A cryogenic test rig for dynamically operated plate–fin heat exchangers. *Chem Ing Tech*. 2021;93(8):1230-1237.
7. Haider P, Freko P, Acher T, Rehfeldt S, Klein H. Influence of inlet configuration and distributor geometry on the performance of cryogenic plate-fin heat exchangers. *Appl Therm Eng*. 2021;195:117197.
8. Klein H, Fritsch P, Haider P, et al. Flexible operation of air separation units. *ChemBioEng Rev*. 2021;8(4):357-374.
9. Zhang Q, Grossmann IE. Planning and scheduling for industrial demand side management: advances and challenges. *Alternative Energy Sources and Technologies*; Cham: Springer; 2016:383-414.
10. Pattison RC, Touretzky CR, Johansson T, Harjunkoski I, Baldea M. Optimal process operations in fast-changing electricity markets: framework for scheduling with low-order dynamic models and an air separation application. *Ind Eng Chem Res*. 2016;55(16):4562-4584.
11. Daryanian B, Bohn RE, Tabors RD. Optimal demand-side response to electricity spot prices for storage-type customers. *IEEE Trans Power Syst*. 1989;4(3):897-903.
12. Zhao S, Ochoa MP, Tang L, Lotero I, Gopalakrishnan A, Grossmann IE. Novel formulation for optimal schedule with demand side management in multiproduct air separation processes. *Ind Eng Chem Res*. 2019;58(8):3104-3117.
13. Zhang Q, Sundaramoorthy A, Grossmann IE, Pinto JM. A discrete-time scheduling model for continuous power-intensive process networks with various power contracts. *Comput Chem Eng*. 2016;84:382-393.
14. Mitra S, Grossmann IE, Pinto JM, Arora N. Optimal production planning under time-sensitive electricity prices for continuous power-intensive processes. *Comput Chem Eng*. 2012;38:171-184.
15. Kelley MT, Baldick R, Baldea M. Demand response scheduling under uncertainty: chance-constrained framework and application to an air separation unit. *AIChE J*. 2020;66(9):e16273.
16. Obermeier A, Windmeier C, Esche E, Repke JU. A discrete-time scheduling model for continuous power-intensive processes considering fatigue of equipment. *28th European Symposium on Computer Aided Process Engineering, Vol. 43 of Computer Aided Chemical Engineering*. Elsevier; 2018:955-960.
17. Obermeier A, Windmeier C, Esche E, Repke JU. A discrete-time scheduling model for power-intensive processes taking fatigue of equipment into consideration. *Chem Eng Sci*. 2019;195:904-920.
18. Obermeier A, Vollmer N, Windmeier C, Esche E, Repke JU. Generation of linear-based surrogate models from non-linear functional relationships for use in scheduling formulation. *Comput Chem Eng*. 2021; 146:107203.
19. Cao Y, Swartz CLE, Baldea M, Blouin S. Optimization-based assessment of design limitations to air separation plant agility in demand response scenarios. *J Process Control*. 2015;33:37-48.
20. Mitra S, Pinto JM, Grossmann IE. Optimal multi-scale capacity planning for power-intensive continuous processes under time-sensitive electricity prices and demand uncertainty. Part I: modeling. *Comput Chem Eng*. 2014;65:89-101.
21. Karwan MH, Keblis MF. Operations planning with real time pricing of a primary input. *Comput Oper Res*. 2007;34(3):848-867.
22. Basán NP, Cóccola ME, Dondo RG, Guarnaschelli A, Schweickardt GA, Méndez CA. A reactive-iterative optimization algorithm for scheduling of air separation units under uncertainty in electricity prices. *Comput Chem Eng*. 2020;142:107050.
23. Schäfer P, Schweidtmann AM, Mitsos A. Nonlinear scheduling with time–variable electricity prices using sensitivity-based truncations of wavelet transforms. *AIChE J*. 2020;99(10):e16986.
24. Kelley MT, Baldick R, Baldea M. An empirical study of moving horizon closed-loop demand response scheduling. *J Process Control*. 2020;92: 137-148. Accessed 24 March 2022. https://www.sciencedirect.com/science/article/pii/S0959152420302183
25. Tsay C, Kumar A, Flores-Cerrillo J, Baldea M. Optimal demand response scheduling of an industrial air separation unit using data-driven dynamic models. *Comput Chem Eng*. 2019;126:22-34. Accessed 24 March 2022. http://www.sciencedirect.com/science/article/pii/S0098135418313371
26. Tsay C, Cao Y, Wang Y, Flores-Cerrillo J & Baldea M. Identification and online updating of dynamic models for demand response of an industrial air separation unit. Accessed 24 March 2022. http://arxiv.org/pdf/2009.13999v1.

27. Tsay C, Baldea M. Integrating production scheduling and process control using latent variable dynamic models. *Control Eng Pract*. 2020;94:104201.

28. Caspari A, Offermanns C, Schäfer P, Mhamdi A, Mitsos A. A flexible air separation process: 2. Optimal operation using economic model predictive control. *AIChE J*. 2019;65(11):e16721.

29. Caspari A, Lüken L, Schäfer P, et al. Dynamic optimization with complementarity constraints: smoothing for direct shooting. *Comput Chem Eng*. 2020;139:106891.

30. Caspari A, Faust JMM, Schäfer P, Mhamdi A, Mitsos A. Economic nonlinear model predictive control for flexible operation of air separation units. *IFAC-PapersOnLine*. 2018;51(20):295-300.

31. Schulze JC, Caspari A, Offermanns C, Mhamdi A, Mitsos A. Nonlinear model predictive control of ultra-high-purity air separation units using transient wave propagation model. *Comput Chem Eng*. 2021;145:107163.

32. Caspari A, Tsay C, Mhamdi A, Baldea M, Mitsos A. The integration of scheduling and control: top-down vs. bottom-up. *J Process Control*. 2020;91:50-62.

33. Vinson DR. Air separation control technology. *Comput Chem Eng*. 2006;30(10–12):1436-1446.

34. Blum N, Krespach V, Zapp G, Oehse C, Rehfeldt S, Klein H. Investigation of a model-based deep reinforcement learning controller applied to an air separation unit in a production environment. *Chem Ing Tech*. 2021;93(12):1937-1948.

35. Engl G, Kröner A, Kronseder T, von Stryk O. Numerical simulation and optimal control of air separation plants. In: Bungartz HJ, Durst F, Zenger C, eds. *High Performance Scientific and Engineering Computing Lecture Notes in Computational Science and Engineering*. Springer; 1999:221-231.

36. Kröner A, Kronseder T, Engl G, Stryk OV. Dynamic optimization for air separation plants. In: Gani R, Jørgensen SB, eds. *European Symposium on Computer Aided Process Engineering, Vol. 9 of Computer-Aided Chemical Engineering*. Elsevier; 2001:433-438.

37. Caspari A, Fahr SR, Offermanns C, Mhamdi A, Biegler LT, Mitsos A. Optimal start-up of air separation processes using dynamic optimization with complementarity constraints. *30th European Symposium on Computer Aided Chemical Engineering, Vol. 48 of Computer Aided Chemical Engineering*. Elsevier; 2020:1147-1152.

38. Wunderlich B. *Entwicklung eines druckgetriebenen dynamischen Kolonnenmodells zur Erhöhung der Flexibilität von kryogenen Luftzerlegungsanlagen* Dissertation. KIT Scientific Publishing; 2018.

39. Rößler F, Thomas I, Freko P, Rehfeldt S, Klein H. Dynamic simulation with digital twins of heat exchangers. *2020 Virtual AIChE Annual Meeting*; AIChE; 2020.

40. Kender R, Rößler F, Wunderlich B, et al. Application of a digital twin of an air separation unit with argon production. *2020 Virtual AIChE Annual Meeting*; AIChE; 2020.

41. Miller J, Luyben WL, Belanger P, Blouin S, Megan L. Improving agility of cryogenic air separation plants. *Ind Eng Chem Res*. 2008;47(2):394-404.

42. Cao Y, Swartz CLE, Flores-Cerrillo J. Preemptive dynamic operation of cryogenic air separation units. *AIChE J*. 2017;63(9):3845-3859.

43. Cao Y, Swartz CLE, Baldea M. Design for dynamic performance: application to an air separation unit. *American Control Conference (ACC)*. IEEE; 2011:2683-2688.

44. Cao Y, Swartz CLE, Flores-Cerrillo J. Optimal dynamic operation of a high-purity air separation plant under varying market conditions. *Ind Eng Chem Res*. 2016;55(37):9956-9970.

45. Schäfer P, Caspari A, Kleinhans K, Mhamdi A, Mitsos A. Reduced dynamic modeling approach for rectification columns based on compartmentalization and artificial neural networks. *AIChE J*. 2019;65(5):e16568.

46. Caspari A, Offermanns C, Ecker AM, et al. A wave propagation approach for reduced dynamic modeling of distillation columns: optimization and control. *J Process Control*. 2020;91:12-24.

47. Cao Y, Swartz CLE, Flores-Cerrillo J, Ma J. Dynamic modeling and collocation-based model reduction of cryogenic air separation units. *AIChE J*. 2016;62(5):1602-1615.

48. Stichlmair J, Klein H, Rehfeldt S. *Distillation: Principles and Practice*. 2nd ed. American Institute of Chemical Engineers; 2021.

49. Singla R, Chowdhury K. Comparisons of thermodynamic and economic performances of cryogenic air separation plants designed for external and internal compression of oxygen. *Appl Therm Eng*. 2019;160:114025.

50. Rößler F, Krumova V, Gewald S, et al. Hazard analysis of fixed-tube-sheet shell-and-tube heat exchangers. *Chem Ing Tech*. 2022.

51. Thomas I, Wunderlich B, Grohmann S. Pressure-driven dynamic process simulation using a new generic stream object. *Chem Eng Sci*. 2020;215:115171.

52. Jiang Y, Yin S, Dong J, Kaynak O. A review on soft sensors for monitoring, control, and optimization of industrial processes. *IEEE Sens J*. 2021;21(11):12868-12881.

53. Graziani S, Xibilia MG. Deep learning for soft sensor design. *Development and Analysis of Deep Learning Architectures*. Springer; 2020:31-59. doi:10.1007/978-3-030-31764-5_2

54. Lin B, Recke B, Knudsen JKH, Jørgensen SB. A systematic approach for soft sensor development. *Comput Chem Eng*. 2007;31(5–6):419-425.

55. Kadlec P, Gabrys B, Strandt S. Data-driven soft sensors in the process industry. *Comput Chem Eng*. 2009;33(4):795-814.

56. Moll A. Air distillation. In: Górak A, ed. *Distillation: Operation and Applications*. Elsevier/Acad. Press; 2014:255-295.

57. Skogestad S. Probably the best simple PID tuning rules in the world. *Proceedings of AIChE Annual Meeting, Paper 276h, Reno, NV*; AIChE; 2001.

58. Häring HW. The air gases nitrogen, oxygen and argon. In: Häring HW, ed. *Industrial Gases Processing*. Wiley-VCH Verlag; 2008:9-109.

59. Hausen H, Linde H. *Tieftemperaturtechnik: Erzeugung sehr tiefer Temperaturen, Gasverflüssigung und Zerlegung von Gasgemischen. Zweite, völlig neubearbeitete auflage*. Springer Berlin Heidelberg; 1985.

60. Linde GmbH Merchant and Packaged Gases, Gases & Applications; 2020. Accessed 24 March 2022. https://www.linde-gas.com/en/images/0000378_C_HiQ_Gas_and_applications_handbook_branding_update_V2_tcm17-168809.pdf

61. Deuflhard P, Hohmann A. *Numerische mathematik 1: Eine algorithmisch orientierte einführung. 4, überarbeitete und erweiterte auflage ed. de Gruyter Lehrbuch*. Walter de Gruyter; 2008. Accessed xxxx.

62. Edmister WC. Design for hydrocarbon absorption and stripping. *Ind Eng Chem*. 1943;35(8):837-839.

63. Ecker AM, Thomas I, Häfele M, et al. Development of a new column shortcut model and its application in process optimisation. *Chem Eng Sci*. 2019;196:538-551.

64. Kronseder T. *Towards Nonlinear Model-Based Online Optimal Control of Chemical Engineering Plants: Parameterised Controls and Sensitivity Functions for Very Large-Scale Index-2 DAE Systems with State Dependent Discontinuities: Zugl.: Darmstadt, Techn. Univ., Diss., 2002, Vol. 977 of Fortschritt-Berichte VDI Reihe 8, Meß-, Steuerungs-Und Regelungstechnik. Als Ms. Gedr Ed*. VDI-Verl; 2003.